UNIVERSITÁ DEGLI STUDI DI PARMA

Dipartimento di Biologia Evolutiva e Funzionale
Sezione Fisiologia

TESI DI DOTTORATO DI RICERCA IN
"FISIOPATOLOGIA SISTEMICA"
(XXII ciclo)

ELECTRICAL COMPETENCE OF THE INFARCTED HEART FOLLOWING STEM CELL BASED REGENERATIVE THERAPY, IN A RAT MODEL.

Coordinatore:

Chiar.mo Prof. Ezio Musso

Tutore: **Dottorando:**

Chiar.mo Prof. Ezio Musso **Dot.Leonardo Bocchi**

ANNI 2007 - 2010

INDEX

Introduction pag. 3

Figures pag. 13

Materials and Methods

Protocol A: Mobilization of CPCs by GF injection (HGF + IGF1), in chronic myocardial infarction. pag. 16

Protocol B: Mobilization of CPCs by HMGB1 injection, in acute myocardial infarction. pag. 33

Figures and Tables pag. 37

Results

Protocol A pag. 43

Figures and Tables of protocol A pag. 52

Protocol B pag. 69

Figures and Tables of protocol B pag. 71

Discussion pag. 74

References pag. 85

Introduction

Cardiac function, cell death and cell proliferation.

Heart diseases represent the most frequent cause of death in the western world and ventricular fibrillation is the main cause of sudden death in patients who have had a heart attack, killing about 15% of patients within three years of their attack (*Gheorghiade M et al 1998; Kjekshus J 1990*). Many heart diseases result from myocyte loss in the absence of appropriate myocardial repair which leads to progressive heart failure and cardiovascular insufficiency. During the last decade many investigators attempted to modify the ratio "cardiac tissue damage/repair" by means of stem cell based regenerative therapies (*Marbán E et al 2010*).

General properties of stem cells.

Stem cells can be classified by their ability to divide and to produce differentiated cells (Fig. 1). Totipotent cells have a total differentiation capacity. They can divide and produce all the different types of cells in an organism. Totipotent cells can specialize into pluripotent cells that can give rise to most of the tissues necessary for fetal development. The pluripotent cells have the potential to differentiate into multipotent cells. Stem cells can also be classified into adult stem cells (ASC) and embryonic stem cells. A typical ASC is one which, on division, results in one daughter cell that can further differentiate and replenish a whole compartment, while the other cell remains fully self-renewing. The ultimate fate of progeny is the generation of a functionally competent mature cell (*Fuchs E et al 2000*). This model of cell growth has been clearly established in the hematopoietic system. However, it is commonly applied to all self-renewing organs.

Stem cells and the heart.

In the past few years the ability of stem cells to regenerate tissues has been clearly documented. Specifically, experimental observations have shown the plasticity of stem cells indicating that in appropriate conditions stem cells can repair a damaged tissue independently from their origin (*Lagasse E et al. 2000; Jakson KA et al. 1999; Fallon J et al. 2000; Orlic D et al. 2001a; Orlic D et al. 2001b; Kocher AA et al. 2001; Condorelli G et al. 2001*). In this respect adult stem cells obtained from bone marrow may turn into heart and brain or, viceversa, brain and muscle derived stem cells may generate bone marrow (*Reynolds BA e al. 1992; Johansson CB et al. 1999a; Johansson CB et al. 1999b; Clarke DL et al. 2000; Kondo T et al. 2000; Horner PJ et al. 2000; Arvidsson A et al. 2002; Monje ML et al. 2002; Beltrami AP et al. 2003; Oh H et al. 2003*).

Recently, a major paradigm shift has taken hold of the cardiovascular community fuelled by the discovery that stem cells have the capacity to differentiate into the three major cell types of the myocardium: smooth muscle, endothelial, and cardiomyocyte (Quaini *F et al. 2002; Beltrami AP et al. 2003; Urbanek K et al. 2003*). The persistence of this observation through independent validation in multiple laboratories throughout the world bodes well for the potential of this area to have a major impact upon cardiovascular research (*Boheler KR et al. 2002; Hierlihy AM et al. 2002; Oh H et al. 2003*). Despite several disputes regarding frequency, the prevailing opinion is that such transdifferentiation events do occur (*Anversa P et al. 2002; Balsam LB et al. 2004; Murry CE et al. 2004; Chien KR 2004; Anversa P et al. 2004*). In the past few years, coincident efforts by several groups have demonstrated integration of stem cells into the intact heart (*Malouf NN et al. 2001; Jackson KA et al. 2001; Orlic D*

et al. 2001a; Behfar A et al. 2002). Some studies have observed repopulation of damaged myocardium by bone marrow-derived stem cells that confer improved hemodynamic function (*Orlic D et al. 2001a; Orlic D et al. 2001c*). Thus the question no longer appears to be whether cardiomyocyte replacement occurs, but rather what are the characteristics of the progenitor population, how efficiently can such cells integrate into the functioning myocardium, and whether the process can be manipulated by genetic or biochemical techniques to potentiate the regenerative properties of these cells.

Controversies and feasibility of cardiac stem cell therapy.

Sorting out the specifics of much of the current debate in cardiac stem cell research is clouded by multiple controversies. First, estimates vary widely with regard to the capacity of donated cells to survive and subsequently integrate into host tissue. Second, skeptics raised concerns over fusion between donated cells and the adopted home tissue creating a chimeric DNA that could masquerade as integration. Third, there is an issue of whether donated stem cells promote recruitment of endogenous progenitors to assist in regeneration. Fourth, the influence of endogenous factors such as cytokines, growth factors, and the local cellular milieu upon stem cells remains poorly understood (*Terada N et al. 2002; Ying QL et al. 2002; Vassilopoulus G et al. 2003; Wang X et al. 2003; Spees JL et al. 2003; Nygren JM et al. 2004; Alvarez Dolado M et al. 2003; Oh H et al. 2003; Shi D et al. 2004*). Resolution of these key issues will ultimately determine the efficacy and feasibility of stem cell therapy as an interventional approach to repair damaged or failing myocardium.

Electrical and mechanical competence of the newly formed myocardial tissue.

Most stem cell treatments have been found to result in different degrees of amelioration of the mechanical performance of the heart. However, in order for cell therapy to be widely clinically applicable, the optimal cell has to be compatible both mechanically and electrically with the host myocardium. Establishing appropriate electrical connections among newly formed myocytes and surrounding, spared myocytes is of paramount importance for a stable recovery of normal cardiac function. So far, information on this issue is fragmented and no comprehensive study exists aimed at establishing whether the mechanical improvement of cardiac function in patients undergoing stem cell therapy for a given heart condition is associated with an increase, decrease or no changes in the risk of arrhythmias (*Zhang YM et al. 2002; Chang MG et al. 2006; Kuhlmann MT et al. 2006; Mills WR et al. 2007*). Pro-arrhythmia after cell therapy have been attributed to several reasons including: l) heterogeneity of action potentials between the native and the transplanted stem cells; 2) intrinsic arrhythmic potential of injected cells; 3) increased nerve sprouting induced by stem cell injection; and 4) local injury or edema induced by intramyocardial injection (*Makkar RR et al. 2003*). The nature of the injected cell may have the most impact on arrhythmogenesis after transplantation. For instance myoblasts (precursor of skeletal myocytes) and stem cells of different origin differ in their inherent electrophysiologic properties and in their ability to couple electromechanically both among themselves and with host cardiomyocytes. Limited clinical data available thus far suggest that arrhythmias are more likely to occur after myoblast than after stem cell transplantation (*Smits PC et al. 2003; Menasche et al. 2001; Menasche et al. 2003*). Often, the occurrence of arrhythmias is negatively correlated with the ability of the newly formed

tissue to adopt a cardiac fate or to couple electrically with the spared myocardium (*Hahn JY et al. 2008; Roell W et al. 2007*). Finally, limited clinical experience suggests that proarrhythmic effects of cell therapy may be transient (*Makkar RR et al. 2003; Strauer BE et al. 2001; Assmus B et al. 2002; Stamm C et al. 2003; Perin EC et al. 2003; Tse HF et al. 2003*). Nonetheless, because the occurrence of cardiac arrhythmia is highly unpredictable, long-term follow-up studies of cell transplant recipients would seem to be essential for understanding the natural course of stem cell induced arrhythmogenesis, if any.

Cardiac electrical instability in myocardial infarction.

Although the proneness to arrhythmias is increased in both the acute and chronic phase of myocardial infarction the mechanisms of the increased electrical instability are different.

Acute Ischemia. The most important electrical changes that occur upon acute and complete block of coronary circulation include a fall in diastolic membrane potential and initial lengthening, followed by shortening, of the action potential duration, associated with a fall in amplitude and maximal rate of depolarization (*Wit AL et al. 1993*). Additionally, the effective refractory period is prolonged relative to action potential duration and conduction velocity is markedly decreased. Finally excitability, which is initially increased, is subsequently decreased and eventually results in inexcitability. Arrhythmias are a serious complication of acute ischemia. Most experimental studies indicate that a first burst of tachycardia is seen between two and 10 minutes from coronary ligature. Yet evolution into ventricular fibrillation is rare during this phase generally termed phase Ia. This pattern is followed by a 10 minute period of relative quiescence. A second phase (phase Ib) of arrhythmias appears between 20 and

30 minutes from occlusion. The percentage of animals showing these arrhythmias is less than in phase Ia but the evolution towards ventricular fibrillation and death is more frequent (*Smith WTt et al. 1995*).

Chronic Infarct. Ventricular myocytes surviving an acute period of ischemia undergo a number of adaptations that reflect in specific electrophysiological features. Crucial changes also occur in the extracellular matrix. Adaptation is not restricted to the infarcted zone but involves peri-infarct myocytes and cells remote from the infarct zone. When the infarct is in the left ventricle, important alterations also occur in the right ventricle presumably because of a neurohumoral activation which produces modulating factors that appears in the circulation and influences the whole heart. Arrhythmias are a frequent complication of healing (hours to 2 weeks) and healed (weeks to months) infarct. During the healing process following an infarct electrophysiological modifications occur in both subepicardial myocytes and subendocardial Purkinje fibres adjacent to the infarct border (*Boyden Pa et al. 1995; Pinto JM et al. 1999*). In addition conduction velocity is slowed down in subepicardial cells overlaying the necrotic area and critical defects are found in cell connections and gap junctions. Published data indicate that at 3-5 days post-infarct inducibility of tachycardias is closely related to the disorganisation of the gap junctions extending through the entire thickness of the subepicardial layers. In healed myocardial infarction (2 weeks and several months) adapative processes are not limited to cells in the infarct zone and to cells close to the scar. Electrical abnormalities also occur in cells remote to the scar and these changes are different from the alterations in the adjacent cells. Infarct and peri-infarct cells are characterized by marked regional differences involving action potential duration, excitability, and refractoriness and its dispersion. Also, irregularities in gap junctions

which started already during the healing phase become more pronounced. Concomitantly with reduction in gap junction coupling between the cells other fundamental alterations occur in the extracellular spaces with development of microfibrosis between the cells. Propagation is impaired and may follow a zig-zag pattern, especially when an extra-systole is generated (*Peters NS et al. 1997*). The reported changes in gap junction, in their regional distribution and the development of extracellular fibrosis have important consequences for the inducibility and persistence of arrhythmias. Finally, cells at a distance from the scar are characterized by a marked hypertrophy, as shown by morphometric and membrane capacitance indexes, thus increasing electrical instability

Resident cardiac progenitor cells (CPCs) for heart repair.

The heart contains several cohorts of resident cardiac progenitor cells (CPCs) which have been characterized by different groups (*Beltrami AP et al. 2003; Oh H et al. 2003, Martin CM et al. 2004, Messina E et al. 2004, Laugwitz KL et al. 2005, Limana F et al. 2007, Davis DR et al. 2010*) and are considered to be responsible for tissue homeostasis (*Quaini F et al. 2002*). Because CPCs are intrinsically programmed to generate myocardium, they appear best suited for the complex task of reconstituting tissue that is lost with a myocardial infarction (*Chamuleau SA et al. 2009*) and restoring the blood supply in the damaged area (*Dawn B et al. 2005*). These properties of CPCs would be expected to improve the organization and functional integration of newly formed tissues with the spared tissue, minimizing heterogeneous electrical remodeling and poor intercellular coupling occurring with numerous cardiac regenerative treatments (*Hahn JY et al 2008; Wang D et al. 2010*). Thus, mending of the heart promoted by CPCs can be an appropriate substrate to explore the proarrhythmic or antiarrhythmic

consequences of stem cell based myocardial regeneration. CPCs have been reported to express c-Met and insulin-like growth factor-1 (IGF-1) receptors and synthesize and secrete the corresponding ligands, hepatocyte growth factor (HGF) (which mobilizes CPCs) and IGF-1 (which promotes their survival and proliferation) (*Urbanek K et al. 2005*). In infarcted hearts of dogs (*Linke A et al. 2005*), mice (*Urbanek K et al. 2005*) and rats (*Rota M et al 2008*), the intramyocardial injection of HGF and IGF-1 enhanced the translocation of CPCs from the surrounding myocardium to the dead tissue and their viability and growth within the damaged area, fostering cardiac regeneration and improving mechanical function. Accordingly, one would expect that activating the lineage commitment and progeny formation of resident CPCs, via the HGF/IGF-1-receptor systems, can also ameliorate the electrical competence of chronic myocardial infarction. Importantly, post-MI ventricular remodeling contributes to end stage heart failure (*Gheorghiade M et al. 1998*), and lethal arrhythmias are responsible for up to half the deaths in heart failure (*Kjekshus J 1990*).

Recently, it has been shown that High-Mobility Group Box-1 (HMGB1) protein, a mediator of the inflammatory response, when administered to CPCs, both in vitro and in vivo, modulates their function. Additionally, despite its primary inflammatory role, HMGB1-dependent signaling has protective effects in acute myocardial ischemia. In fact, it has been found that HMGB1 blockade leads to exaggerated scarring and more severe ventricular dilation in acute MI (*Kohno et al. 2009*). Injection of HMGB1 in a mouse model of myocardial infarction was found to promote c-kit+ cell proliferation and enhanced myocardial regeneration (*Limana et al. 2005*). Direct and indirect effects have been proposed to account for the HMGB1-induced CPC proliferation. In fact c-kit+ cells express RAGE (*Limana et al. 2005*) and respond to HMGB1; further, cardiac

stromal cells exposed to HMGB1 secrete a variety of pro-inflammatory and pro-angiogenic cytokines that also modulate CPC function (*Rossini et al. 2008*). Taken together, these results suggest that inflammatory modulation and pro-repair signaling by HMGB1 converge into an integrated pathway causing CPC activation at early stages after ischemia, followed by attenuation of the inflammatory machinery and prevention of ventricular remodeling at later stages. So far no data have been obtained on the electrophysiological consequences of cardiac repair mediated by CPCs activation via HMGB1 intramyocardial delivery. Although the efficacy of HMGB1 in acute ischemia has not been fully elucidated we believe that this analysis would provide important data in order to evaluate the electrical competence of the regenerated heart in the early stages of myocardial injury.

Aim of the study. By following an approach from the intact animal to tissue, cellular, and molecular levels we tested the hypothesis that mobilization of CPCs: (i) either through locally delivered Hepatocyte Growth Factor and Insulin-Like Growth Factor-1 to repair chronic myocardial infarction (Protocol A, see Table 1), (ii) or through intramyocardial administration of HMGB1 to restore cardiac function in acute ischemia (Protocol B, see Table 2), lowers the proneness to arrhythmias.

Figures

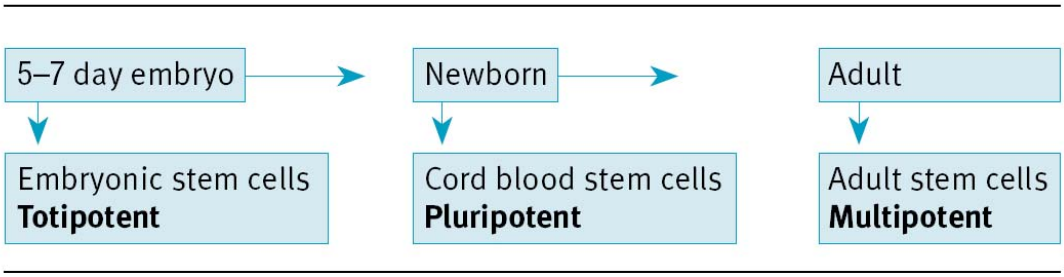

Fig. 1. **Differentiation potential of stem cell lineages.**

Materials and Method

Protocol A: Mobilization of CPCs by GF injection (HGF + IGF1), in chronic myocardial infarction.

A1. Animals and housing.

All experimental procedures were approved by the Veterinarian Animal care and use Committee of Parma University and conformed with the National Ethical Guidelines (Italian Ministry of Health; D.L.vo 116, January 27, 1992) and the Guide for the Care and Use of Laboratory Animals (NIH publication no. 85–23, revised 1996).

The study population consisted of 133 rats male Wistar rats (*Rattus norvegicus*) bred in our departmental animal facility, aged 12-14 wk, weighing 300-350 g. The animals were kept in single-sex groups of four individuals from weaning (4wk after birth) until the onset of the experiments, in a temperature-controlled room at 20–24°C, with the light on between 7.00 AM and 7.00 PM. The bedding of the cages consisted of wood shavings, and food and water were freely available.

The animals were subjected either to myocardial infarction (MI group) or sham operation (SO group). Four weeks later, all animals were treated with growth factors (GFs) or vehicle (V) and assigned to the following groups: MI+GF, MI+V and SO+V. GFs were Hepatocyte Growth Factor (HGF) and Insulin-Like Growth Factor-1 (IGF-1).

Owing to the multifactorial nature of arrhythmogenesis in myocardial infarction, all animals with anatomically documented MI were used in the study, even if infarct size was small.

A2. General outlines of the experimental protocol A.

The experimental design and measurements performed in the study are summarized in Table 1.

Sixty rats were chronically instrumented with a Telemetry-ECG system (TE rats, Table 1). After one week, a 30-minute continuous baseline ECG was recorded to rule

out the presence of spontaneous arrhythmias. The animals were then subjected either to myocardial infarction (MI group, 45 rats) or to sham operation (SO group, 15 rats) and, four weeks later, investigated for vulnerability to arrhythmias and cardiac mechanical performance by (i) telemetry-ECG recording in baseline condition and stress-induced autonomic stimulation (social stress procedure) and (ii) echocardiograpy. Afterwards, all rats were re-operated on and intra-myocardial injections of growth factors or vehicle were performed (MI+GF group, 22 rats; MI+V, 23 rats; SO+V, 15 rats). Simultaneously with GF or V (GF/V) administration, selected subgroups of MI+GF (n=14) and MI+V rats (n=11) were also treated with 5-Bromo-2'-deoxycytidine (BrdC), to evaluate the cumulative amount of cell proliferation. Two weeks later, vulnerability to arrhythmias and cardiac mechanical function were re-determined by a new series of telemetry-ECG and echocardiographic measurements and, subsequently, hemodynamic data were invasively collected. Finally, at sacrifice, the heart was perfusion fixed for anatomical studies (all TE rats), and morphometric and immunohistochemical studies (selected subgroups of animals).

In 43 additional rats, assigned to the MI+GF (n=24) or MI+V (n=19) groups, further electrophysiological investigations were performed by Epicardial Multiple-lead recording (EM rats, Table 1). In all animals, four weeks after MI, 25-64 unipolar electrograms (EGs) were collected from as many sites of the infarcted epicardial surface and surrounding areas. EGs were recorded during sinus rhythm or specific pacing protocols for determining basic cardiac electrophysiological properties (conduction velocity, excitability and refractoriness) as well as dispersion of refractoriness and QT interval duration. Subsequently, growth factors or vehicle were administered to the proper subgroups. Two weeks later, the animals were re-operated on, all

electrophysiological measurements were repeated and, at sacrifice, the heart was perfusion fixed for identifying the infarcted portion of the ventricle.

Finally, in 30 rats assigned to the MI+GF, MI+V and SO+V groups, two weeks after GF/V injection the heart was excised and frozen for Molecular Biology analyses (MB rats, Table 1) which included electrophoretic and immunoblot assays (5 MI+GF and 5 MI+V animals) and quantitative RT-PCR measurements (9 MI+GF, 8 MI+V and 3 SO+V animals).

The details of the procedures employed in the study are described below.

A3. Telemetry-ECG recording.

A3.1 ECG telemetry System.

The radiotelemetry system consisted of a miniaturized transmitter for telemetry ECG recording (25 x 15 x 8 mm; model TA11CTA-F40, Data Sciences, St Paul, MN, USA) and a receiver (model CTR85-SA, Data Sciences, St Paul, MN, USA) which was placed under the experimental cage during the recording sessions (Fig. 2)

A3.2 Chronic instrumentation for telemetry-ECG recording.

The telemetry ECG transmitter was chronically implanted according to a surgical procedure previously published (*Sgoifo A et al. 1996*). Briefly, the animals were anesthetized with ketamine chloride 40mg/kg ip (Imalgene, Merial, Milano, Italy), plus medetomidine hydrochloride 0.15 mg/kg ip (Domitor, Pfizer Italia S.r.l., Latina, Italy). A ventral celiotomy was performed and the body of the transmitter (25x15x8 mm) was placed in the abdominal cavity. One recording lead was fixed to the dorsal aspect of the xiphoid process, close to the apex of the heart. The other lead was subcutaneously tunneled on the thorax toward the upper insertion of the sternohyoid

muscle. Here, the wire was formed into a U shape, pushed under the muscle and then along the trachea into the anterior mediastinum, to get the tip of the recording lead close to the right atrium. Finally, the muscle and skin layers were separately sutured.

After surgery, all animals were given atipamezole hydrochloride 0.15 mg/kg im (Antisedan, Pfizer Italia S.r.l.), flunixin 5 mg/kg im (Finadyne, Schering-Plough S.p.a, Milano, Italy), gentamicine sulphate 10 mg/kg im (Aagent, Fatro, Milano, Italy), and kept warm with infrared lamp radiation. Antibiotic therapy was continued in the following three days while the animals were individually housed.

A3.3 Social stress procedure and telemetry-ECG data acquisition and processing.

Social stress was obtained by resident–intruder test paradigm (*Martinez M et al, 1998*) which consists of introducing the instrumented animal (intruder) into the territory of an unfamiliar conspecific male (resident) belonging to an aggressive wild strain of rats (Rattus norvegicus, Wild Type Groningen, WTG). All experimental session were carried out during the light phase, between 9.00 AM and 1 PM. Each session consisted of two successive 15-min telemetry ECG recordings which were performed while the instrumented animal was respectively: (i) left alone and undisturbed in its home cage (baseline conditions) and (ii) exposed to the social stress procedure (test period). During the entire recording session, the telemetry ECG receiver (Fig. 2) was placed under the experimental cage. ECGs, provided as analog signals at the output of the receiver, were continuously monitored on an oscilloscope and simultaneously routed to a personal computer via an analog-to-digital conversion board (12 bits, 1000 Hz sampling rate, Fig. 2). A real-time acquisition program allowed the digital data to be continuously recorded and stored on hard disk for off-line processing. The data were then analyzed by using a custom made software package for measuring R–R interval, interactively detecting

ventricular rhythm disturbances and computing heart rate-based-indices of autonomic input to the heart. The indices included the standard deviation of R-R interval (SD_{RR}) and the square root of the mean of the squared differences between adjacent R-R interval (r-MSSD) taken respectively as indices of cardiac sympathovagal balance and vagal input to the heart (*Malik M et al. 1995).* Ventricular arrhythmic events (VAEs) were classified as follows: (i) PVBs: isolated premature ventricular beats, and (ii) salvos: episodes of two or three consecutive PVBs (*Walker MJA et al. 1988*).

A4. Myocardial infarction.

Rats under ketamine-medetomidine anaesthesia were intubated and artificially ventilated (Rodent ventilator UB 7025, Ugo Basile, Comerio, Italy). With the aid of a dissecting microscope, a thoracotomy via the third-left intercostal space was performed and a 5-0 silk suture was passed with a tapered needle under the left anterior descending coronary artery, 2-3 mm from the edge of the left auricle, and tied securely. The development of a pale colour in the distal myocardium on ligature, as noted by visual inspection, was taken as index of successful performance of coronary occlusion. The chest was then closed in layers, and a small catheter was introduced in the thorax to evacuate air and fluids. The rats were given atipamezole hydrochloride, removed from the ventilator, kept warm with infrared lamp radiation and eventually individually housed. Antibiotic therapy was given during the subsequent 3 days, as indicated above. Sham-operated rats were treated similarly, except that the ligature around the coronary artery was not tied.

A5. Intramyocardial injection of HGF+IGF-1 and BrdC delivery.

Four weeks after coronary ligature, left lateral thoracotomy was repeated in all animals under anaesthesia and artificial ventilation as described above. In MI+GF rats six injections with increasing concentrations of HGF (PeproTech EC, London, UK) and constant concentration of IGF-1 (PeproTech EC) were done. The first injection was located near the atria, the second between the atria and the infarct and the last four at opposite sites of the border zone. In MI+V and SO+V rats, corresponding regions of the heart were injected with vehicle. The sterile solution of growth factors contained different concentration of HGF (atria: 50 ng /mL; atria-border zone: 100 ng/mL; opposite sides of border zone: 200 ng/mL) and constant concentration of IGF-1 (200 ng/mL in all six injection sites) diluted in saline (phosphate buffer solution: PBS). In MI+GF rats, Rhodamine microspheres, 2.0 μm in diameter (FluoSpheres, Molecular Probes, Eugene, USA), were added to the solution (v/v 5%) to ensure the successful injection. The volume of each injection was 10 μL.

Simultaneously to the GF/V injection, in selected subgroups of MI+V and MI+GF animals, an osmotic pump (model 2ML4, ALZET, Charles River, Italy) was implanted subcutaneously in the interscapular region for continuous infusion of BrdC (0.6 mol/L; MP Biomedicals Europe, Asse-Relegem, Belgium) with a delivery rate of 2.5 μL/h. Infusion was maintained until the animals were killed (15 days). The long infusion time prompted us to use BrdC rather than BrdU because of the nearly six fold higher solubility of BrdC.

A6. Echocardiographic measurements.

Serial echocardiograms were obtained in rats under ketamine-medetomidine anaesthesia, using a Vivid 7 echocardiography machine (GE Medical Systems, Madison,WI, USA) equipped with 10 - 7 MHz phased array transducers The anterior chest was shaved and the animals were placed in the left lateral decubitus position. Two-dimensional (2-D) and M-mode images were recorded from modified parasternal long axis and parasternal short-axis views. Diastolic and systolic anatomical parameters were obtained from M-mode tracings at the mid-papillary level. The measurements included: (i) end-diastolic and systolic left ventricular diameter (LVEDD and LVSD, respectively); (ii) end-diastolic and end-systolic left ventricular volume (LVEDV, LVESV), and (iii) ejection fraction and fractional shortening (EF, FS). Data were analyzed by an investigator who was blind to the treatment

A7. Hemodynamic studies.

Rats were anesthetized with droperidol + fentanyl citrate (Leptofen, Farmitalia-Carlo Erba, Milan, Italy; 1.5 mg/kg im) which we have found to induce negligible changes in hemodinamic parameters as measured in conscious animal by means of telemetry recording (unpublished data). The right carotid artery was cannulated with a microtip pressure transducer catheter (Millar SPC-320, Millar Houston, TX, USA) connected to a recording system (Power Laboratory ML 845/4 channels, 2Biological Instruments, Besozzo-Varese, Italy) and systolic and diastolic blood pressure were determined. The catheter was then advanced into the left ventricle to measure: (i) left ventricular systolic (LVSP) and end-diastolic pressure (LVEDP) and (ii) maximum rate

of ventricular pressure rise (+dP/dt) and reduction (-dP/dt) in the closed-chest preparation. (software package CHART B4.2).

A8. Epicardial multiple-lead recording

Each rat under ketamine - medetomidine anaesthesia and artificially ventilated was subjected to left thoracotomy. Body temperature was held constant at 37°C by infrared lamp radiation. A 5x5 or 8x8 row and column electrode array, fabricated on a surgical gauze patch, with 1 mm resolution square mesh, was positioned on the infarcted region and the surrounding areas with the upper border of the array just below the site of coronary ligature (Fig. 3a-b). The construction of the electrode array and the multiple lead recording system have been described in detail before (*Macchi E et al. 1998*). The following measurements were carried out:

A8.1 Conduction velocity.

In each experiment, 64 unipolar electrograms (EGs) were recorded during normal sinus rhythm (SR) or ventricular pacing at 8 selected electrodes of the array (Fig. 3c), by near-threshold, ≤1 ms cathodal current pulses, at a frequency slightly higher than spontaneous SR (≈ 300 bpm). During pacing, unipolar EGs were recorded from all the electrodes except at the paced site (Fig. 3d). Activation times were estimated using the instant of the minimum time derivative of unipolar EGs during QRS, and were referenced to QRS onset or stimulus onset. From the activation times of paced beats an activation sequence (isochrone map) was determined where Conduction Velocity (CV) was computed longitudinally (CV_l) and transversally (CV_t) to fiber orientation (Fig. 3e). Specifically, CV_l was evaluated from electrodes distant from the pacing site on the long axis of the elliptical wavefront. CV_t was evaluated from

electrodes on a line perpendicular to the long axis of the elliptical wavefront across the more closely spaced isochrones. It is known that the long axis of the elliptical wavefront is parallel to the local fiber direction at the pacing site (*Taccardi B et al. 2008*)

A8.2 Excitability.

Eight selected electrodes of the array (see above) were initially paced with current pulses of decreasing strength (starting from liminar values) at a constant width of 5 ms till activation failed, thus identifying threshold current (I_{th}). The procedure was repeated with current pulses of progressively shorter width, up to 0.01 ms. The threshold currents as a function of pulse duration define the strength-duration (S-D) curve (Fig. 3f) which is represented by the hyperbolic equation (*Lapicque L 2007*) relating threshold current strength I and pulse duration T:

$$I = Rh\left(1+\frac{Chr}{T}\right)$$

where Rh is the rheobase (i.e. the lowest intensity with infinite pulse duration which succeeds in eliciting a propagated response in excitable tissues) and Chr the chronaxie (i.e. the pulse duration having a threshold intensity of twice Rh). The two parameters which univocally identify the S-D curve, characterize tissue excitability (Fig. 3f).

A8.3 Refractoriness.

At each of the 8 selected electrodes of the array (see above), 10 baseline stimuli (S1), 1 ms width and twice diastolic threshold intensity, were delivered at a pacing cycle length of 300 ms. The S1 pacing sequence was followed by an extra-stimulus (S2) whose delay from previous S1 was first progressively decremented by 10ms steps until capture was lost and then progressively incremented by 2 ms steps till capture was resumed. The longest S1-S2 coupling interval that did not originate ventricular capture

identified the effective refractory period (ERP) at a given electrode site, enabling the characterization of spatial differences in tissue refractoriness.

A8.4 Dispersion of refractoriness.

The degree of dispersion was evaluated by computing ERP dispersion value taken as basic indicator of propensity to re-entrant arrhythmias (*Opthof T et al. 1993).* In an individual animal ERP dispersion was expressed by the standard deviation of the mean ERP at all test sites (*Ogawa S et al. 1991*).

A8.5 QT interval duration.

In each animal, the duration of QT and corrected QT interval (normalized to cycle length: QTc) (*Mitchell GF et al. 1998*) was measured from the root mean square (RMS) signal computed from all the 8x8 EGs and represented the average of 4 randomly selected beats. The RMS provides a composite measure of all electrical activity as a single positive-magnitude average of signals obtained from multiple unipolar EGs simultaneously (*Fuller MS et al. 2000*), greatly improving the signal to noise ratio. QT duration was computed as the interval between QRS onset and the time of the minimum of the first derivative of RMS signal, during the descending limb of T-wave (*Lux RL et al. 2006*).

A9. Cardiac anatomy.

The abdominal aorta was cannulated, the heart was arrested in diastole with injection of $CdCl_2$ solution (100 mmol/L iv), and the myocardium was retrogradely perfused with 10% buffered formalin solution. The left ventricular chamber was filled with fixative at a pressure equal to the in vivo measured systolic pressure.

The heart was then excised and placed in formalin solution (10%) for 24 hours. The right ventricle (RV) and the left ventricle (LV) inclusive of the septum were separately weighed and the volume of the left ventricular myocardium was computed by dividing LV weight by the specific gravity of the tissue (1.06 g/mL). LV chamber length was measured from the apex to the aortic valve. Three 1-mm-thick transverse slices were cut from the base, mid-region, and apex of the LV. The mid-slice was used to measure LV wall thickness and chamber equatorial diameter (Image Pro-plus, Media Cybernetics, Bethesda, USA)**.** The LV chamber volume was computed according to the Dodge equation (*Dodge HT et al. 1969*). The three slices were then embedded in paraffin and from each slice five-micrometer-thick sections were cut and used for morphometric and immunohistochemical analyses.

A10. Morphometrical analysis.

A10.1 Collagen accumulation in the spared LV.

Five-micrometer-thick sections from the equatorial slice of the LV (see above) were stained with Masson's trichrome and analyzed by optical microscopy (magnification 250X) in order to evaluate in the remote spared myocardium: (i) the volume fraction of myocytes, (ii) the volume fraction of fibrosis, and (iii) the numerical density and average cross-sectional area of fibrotic foci. Quantification of myocardial

scarring resulting from focal myocyte cell loss were included in the analysis since foci may represent an important ongoing post-infarction tissue injury. According to a procedure previously described (Stilli D et al. 2007), for each section, a quantitative evaluation of the volume fraction of myocytes and fibrotic tissue was performed in 60 adjacent fields from sub-endocardium, mid-myocardium and sub-epicardium. The measurements were obtained with the aid of a grid defining a tissue area of 0.160 mm^2 and containing 42 sampling points each covering an area of 0.0038 mm^2.

A10.2 Infarct Size.

In MI animals, the area of the damaged tissue from the endocardial to the epicardial layer and the total area of the viable myocardium were measured in the three slices corresponding to the base, mid-region and apex, indicated above. Due to shrinkage of the infarcted region and ongoing myocyte growth and death within the viable myocardium, the computation of the number of lost and remaining myocytes after infarction provides a more appropriate characterization of infarct size and extent of recovery with time**.** The number of myocytes in the LV of control and infarcted hearts was obtained by employing a methodology well-established in our laboratory (*Olivetti G et al. 1991; Orlic D et al. 2001a).* The quotient between the number of myocytes present in the infarcted LVs and the number of LV myocytes in sham-operated animals gives the percentage of myocytes lost after infarction. The percentage of myocytes lost provides a quantitative measurement of infarct size, while the percentage of myocytes left correlates with ventricular function. The newly-formed myocardium in treated hearts was not included in this analysis, in order to evaluate the consequences of coronary ligature on infarct size independently of tissue reconstitution.

A10.3 Myocyte Cell Size.

In sections of 7 SO+V, 10 MI+V and 12 MI+GF hearts obtained from as many randomly selected TE rats, the cross-sectional area of myocytes was morphometrically determined by measuring the cell diameter, at the nucleus level, in transversally oriented myocytes**.** For each heart, 120 to 250 cellular measurements were performed.

A11. Immunohistochemical analysis.

Five-micrometer thick sections (see above), obtained from rat hearts treated with BrdC and exhibiting comparable infarct size, were analyzed to determine: (i) the expression and spatial distribution of connexin43 (Cx43) and N-cadherin, (ii) the incidence of c-kit+ CPCs, and (iii) the fraction of nuclei labeled by BrdU, in the infarcted, peri-infarcted and remote LV myocardium. The quantification of BrdU labeling in arterioles was not included in the study because the procedure does not allow us to assess the fraction of newly formed structures, which are constituted by a multiple layer of cells. BrdU, c-kit, Cx43 and N-cadherin labeling was detected by immunofluorescence. LV sections were incubated with the primary antibody (monoclonal mouse anti-BrdU antibody, dilution 1:20, Dako, Glostrup, Denmark; rabbit polyclonal anti-c-kit antibody, dilution 1:20, Santacruz Biotecnology, Inc, Santa Cruz, CA, USA; mouse monoclonal anti-Cx43 antibody, dilution 1:250, Chemicon, Temecula, CA, USA; rabbit polyclonal anti-N-cadherin antibody, dilution 1:200, Calbiochem, San Diego, CA, USA). Myocytes, smooth muscle cells and endothelial cells were identified by staining the same sections respectively with monoclonal mouse anti-asarcomeric actin antibody (anti-α-SARC; dilution 1:30, Dako), monoclonal mouse anti-a-smooth muscle actin antibody (anti-α-SMA; dilution 1:50, Dako), and polyclonal

rabbit anti-vW factor (dilution 1:100, Dako) respectively. FITC-, TRITC- Cy5-conjugated anti-mouse or anti-rabbit secondary antibodies (Jackson Laboratory, Baltimore, PA, USA) were used to detect simultaneously the different epitopes. Nuclei were recognized by DAPI (4',6-diamidino-2-phenylindole) staining. The amount of newly formed myocardium was computed by calculating the number and size of small a-SARC+ myocytes according to a methodology previously employed (*Orlic D et al. 2001a*). The number of resistance arterioles was measured by counting vascular profiles labeled by α-SMA, within the infarcted myocardium.

A12. Electrophoretic and immunoblot analysis.

The infarcted and non-infarcted portions of the LV ventricles were weighed and immediately frozen at -80 °C. For immunoblot assay of Cx43, the fresh ventricular tissue was lysed with 150-200 mL of lysis buffer containing the following (SIGMA, St Louis, MO, USA): protease inhibitor dithiothreitol (0.5 mmol/L), DNase (50 mg/mL), RNase (50 mg/mL), HEPES (10 mmol/L), NaCl (400 mmol/L), EGTA (0.1 mmol/L), glycerol (5%), NP40 (3%). Equivalents of 100-125 mg of protein were separated by 10.5% SDS-PAGE, transferred on nitrocellulose filters and exposed to anti-Cx43 monoclonal mouse antibody (dilution 1:750, Chemicon). Binding sites were detected by peroxidase-conjugated specific anti-mouse IgG (dilution 1:2000, in ECL reagents; Amersham Biosciences**,** Piscataway, NJ, USA). The intensity of the bands representing the connexin protein was quantified using a densitometer (Molecular Dynamics, Sunnyvale, CA, USA) and the data were expressed as optical density units.

A13. Real-Time RT-PCR: Quantification of Kv (α) and accessory subunits.

Immediately after death, the LV and RV were excised from the heart; each sample was frozen in liquid nitrogen, and stored at -80°C. Total RNA from each cardiac sample was isolated and DNasetreated with the RNeasy Fibrous Tissue Mini Kit (Qiagen, Milan, Italy) following the manufacturer's instructions. Isolated RNA was quantified (spectrophotometric absorbance at 260 nm) and purity was confirmed by the A260/A280 ratio. Integrity of total RNA was evaluated by ethidium bromide staining on denaturing agarose gels. RNA samples were stored at -80°C.

A13.1 Reverse transcription.

Single-stranded cDNA was performed by using High Capacity cDNA Reverse Transcription Kit (Applied Biosystems, Foster City, CA, USA) following the manufacturer's instructions. The reverse transcription reaction was performed by incubating a reaction mixture containing: 2 μg RNA, 10X RTBuffer, 10X RT-random primers, 25X dNTP Mix (100 mmol/L), RNase inhibitor, and Multiscribe Reverse Transcriptase in a total of 20 μL 1X reaction buffer. Reverse transcription was performed at 25°C for 10 min, 37°C for 120 min and stopped by incubating at 85°C for 5s.

A13.2. Real-Time RT-PCR.

Expression levels of Kv1.4, Kv4.2, Kv4.3 and KChiP2 genes were investigated using real-time quantitative RT-PCR and TaqMan® probe-based chemistry. When evaluated by the same method, the gene GAPDH showed stable expression in the LV and RV under all of the experimental conditions and was therefore used as endogenous control gene. Primers and probes were obtained from ABI (Applied Biosystems, Foster City, CA, USA) TaqMan Gene Expression Assay catalogue. These assays come in a

20X reaction mix, span an exon-exon junction, and are optimized to give approximately 100% efficiency. The realtime RT-PCR reactions were performed using TaqMan® Gene Expression Master Mix (Applied BioSystems) in a 20 µL reaction volume containing 50 ng of cDNA. All reactions were performed in triplicate and included a negative control. PCR reactions were carried out using an ABI Prism 7500 Sequence Detection System (Applied Biosystems). Cycling conditions were: 2-min at 50°C, 10-min at 95°C, and 40 cycles of 15 s at 95°C and 1-min at 60°C. Relative quantification of mRNA levels was obtained by the 7500 system software, which uses the comparative method (ΔCT).

Protocol B: Mobilization of CPCs by HMGB1 injection, in acute myocardial infarction.

B1. HMGB1 Production. The purified High-mobility group box 1 protein (HMGB1) as well as its inactive truncated form (boxA) were provided by Laboratorio di Patologia Vascolare, Istituto Dermopatico dell'Immacolata, Istituto di Ricovero e Cura a Carattere Scientifico, Rome, Italy.

B2. Animals.

Twenty-three, 4-month old male Wistar rats (*Rattus Norvegicus*) were used in the study. The animals were maintained in groups of 5 individuals and housed in clear makrolon cages measuring 55 X 35 X 20 cm, from weaning until telemetry ECG transmitter implantation. Animals were always kept in a temperature-controlled room at 22–24 °C, with the light on between 7.00 AM and 7.00 PM.

The experimental design and measurements performed in the study are summarized in Table 2.

B3. Surgical procedure for implantation of telemetry ECG transmitter.

All animals were chronically instrumented with a miniaturized telemetry ECG transmitter (Data Sciences), as described under subheading A3 of protocol A.
Myocardial infarction was induced 10 days after surgery.

B4. Myocardial infarction and Protein Injection.

Myocardial infarction was induced in 17 rats, anesthetized with ketamine - medetomidine anaesthesia and artificially ventilated, by following the same procedure described under subheading A4 of protocol A. The remaining 6 animals were sham-

operated. The chest was closed and the animals were allowed to recover. After 4 hours, the animals were re-operated and injected with: (i) 2 μg of purified HMGB1 (7 MI rats, MI+HMGB1 group) diluted in phosphate buffer solution (PBS), or (ii) 2 μg of inactive protein (10 MI rats and 6 sham operated animals: MI+boxA and SO groups). In each MI rat, four injections (5 μL per injection) were made in the viable myocardium bordering the infarcted area, through a 26-gauge needle. Corresponding regions of the left ventricular wall were injected in SO rats (*Limana F et al. 2005*). Cardiac electrical performance was evaluated two weeks after surgery.

B5. Evaluation of cardiac electrical performance: telemetry ECG recording

Two successive 15-min telemetry ECG recordings were performed in baseline conditions and during social stress exposure, as described under subheading A3.3 of protocol A. The data were then analyzed by using a custom made software package for measuring, in the two experimental conditions, the average values of : a) R–R interval, b) R-R interval variability indices (SD_{RR}: standard deviation of R-R interval and r-MSSD: the square root of the mean of the squared differences between adjacent R-R interval), and c) number of ventricular arrhythmic events (VAEs).

B6. Infarct size.

After telemetry ECG recording, the animals were sacrificed. The abdominal aorta was cannulated, the heart was arrested in diastole, and the left ventricular chamber was perfusion-fixed, as described under subheading A9 of protocol A. Then, the left ventricles of MI animals were analyzed to verify the presence and measure the size of myocardial infarction (see also subheading A10.2. of protocol A).

Statistical analysis.

The SPSS statistical package was used (SPSS, Chicago, IL, USA, 17th version). Normal distribution of variables was checked by means of the Kolmogorov-Smirnov test. Statistics of variables normally distributed (all variables except baseline arrhythmias) included mean ± standard error (SE), paired and unpaired Student's t test, and one-way analysis of variance (post-hoc analysis: Games-Howell test and Tukey test when appropriate). Non-parametric statistical tests were used to evaluate differences in the incidence of baseline ventricular arrhythmias among groups (Kruskall-Wallis test and Mann-Whitney U-test), and differences between baseline and stressinduced arrhythmias within each group (Wilcoxon test). Statistical significance was set at $p<0.05$.

Figures and Tables

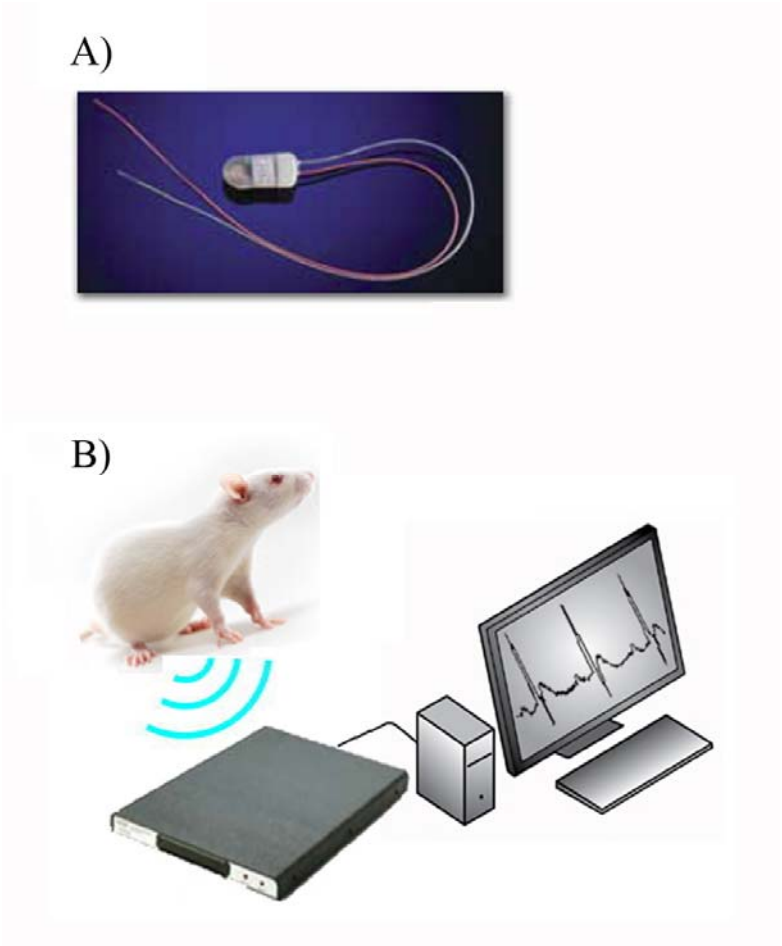

Fig.2. ECG Data acquisition
A- Telemetry ECG transmitter, chronically implanted in each TE animal.
B - Telemetry ECG, provided as analog signal at the output of the receiver, was routed to a personal computer via an analog-to-digital conversion board (12 bits, 1000 Hz sampling rate)

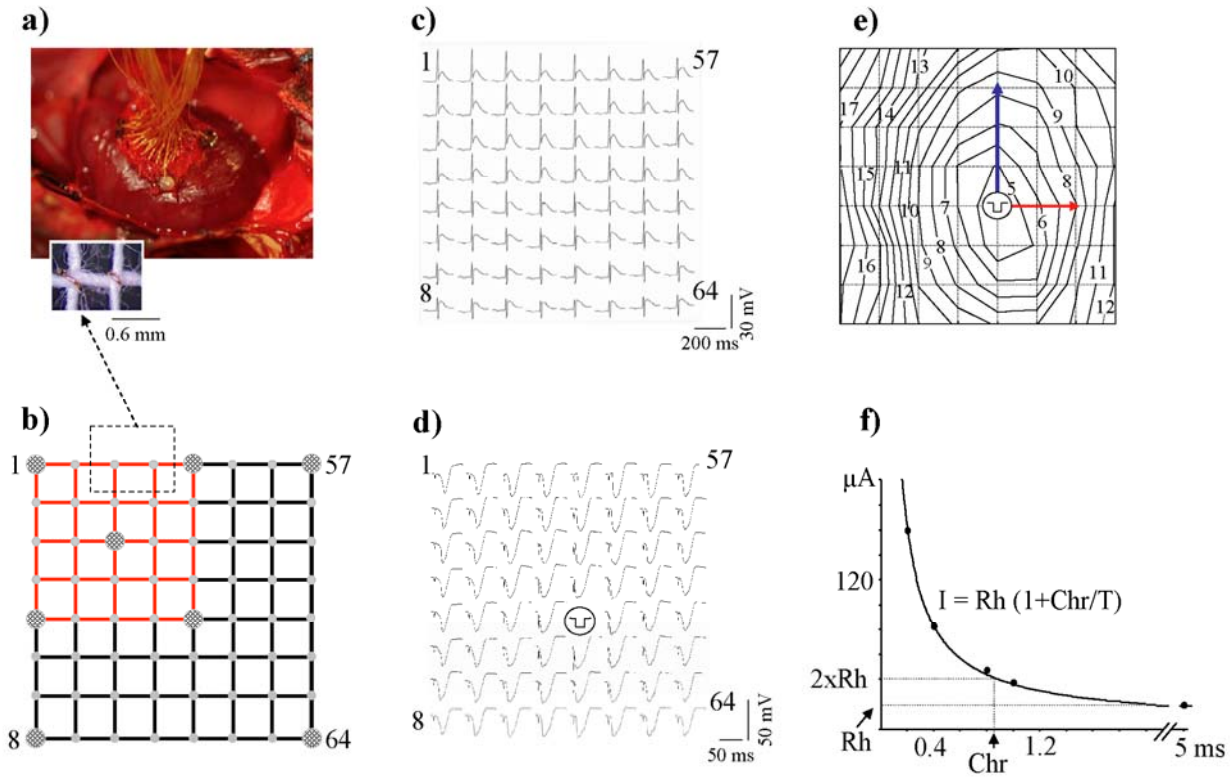

Fig. 3 Epicardial multiple-lead recording: electrode arrays and procedures.
a) Electrode array positioned on the anterior aspect of the left ventricular surface.
b) Schematic representation of the 5x5 (in red) and 8x8 electrode arrays showing the positions (larger circles) of the 5 and 8 selected electrodes used for specific pacing protocols.
c) and **d)**: Unipolar electrograms collected by means of the 8x8 electrode array during normal sinus rhythm (c) and ventricular pacing at the electrode indicated by the pulse symbol (d).
e): example of paced activation isochrone map used for computing conduction velocity longitudinally (blue-arrow) and transversally (red-arrow) to fiber orientation; numbers on each isochrone line indicate the activation time in ms.
f): strength-duration curve obtained in a control rat by plotting pulse threshold current I as a function of pulse duration T (Rh: Rheobase, Chr: Chronaxie).

Table 1. Outline of the experimental protocol A

In vivo studies	day	TE rats (n=60)	EM rats (n=43)	MB rats (n=30)
Chronic instrumentation for telemetry-ECG recording	1	+	-	-
Telemetry-ECG recording in baseline conditions	7	+	-	-
Myocardial infarction	10	+	+	+
Echocardiographic measurements	32	+ (selected subgroups)	-	-
Telemetry-ECG recording during baseline and social stress conditions	36	+	-	-
Epicardial multiple-lead recording	39	-	+	-
Intramyocardial injection of HGF+IGF-1 or vehicle	39	+	+	+
Implantation of an osmotic pump for continuous (two weeks) BrdC delivery	39	+ (selected subgroups)	-	-
Echocardiographic measurements	52	+ (selected subgroups)	-	-
Telemetry-ECG recording during baseline and social stress conditions	54	+	-	-
Epicardial multiple-lead recording	54	-	+	-
Hemodynamic measurements		+ (selected subgroups)	-	-
Sacrifice	60	+	+	+
Post mortem studies				
Anatomical identification of myocardial infarction		+	+	
Cardiac anatomy and infarct size		+	-	-
Morphometric analysis		+ (selected subgroups)	-	-
Immunohistochemical analysis		+ (selected subgroups)	-	-
Electrophoretic and immunoblot analysis		-	-	+ (selected subgroups)
Quantitative RT-PCR measurements		-	-	+ (selected subgroups)

Table 2. Outline of the experimental protocol B

In vivo studies	**days**	**MI+boxA (n=10)**	**MI+HMGB1 (n=7)**	**SO n=6**
Chronic instrumentation for telemetry ECG recording	1	+	+	+
Myocardial infarction	10	+	+	+
Simulate surgery	10			+
Intramyocardial injection of HMGB1 or truncated form (boxA)		+	+	+
Telemetry ECG recording during baseline and social stress	36	+	+	+
Sacrifice	36	+	+	+
Post mortem study				
Infarct size		+	+	

Results

Results of protocol A

1. Telemetry-ECG recording.

1.1. R-R interval and R-R interval variability (SDRR and r-MSSD).

R-R interval, SD_{RR} and r-MSSD during baseline had similar values in all groups or exhibited negligible differences (Table 3). Stress procedure, generally, increased heart rate by about 30% and reduced SD_{RR} and r-MSSD by about 40% and 30% respectively (Table 2)., as a result of the enhanced sympathetic activity brought about by the social challenge (*Martinez M et al. 1998*). The effects of stress were similar before and after GF/V injection in each animal group, suggesting that growth factor administration did not have affect to autonomic input to the heart.

1.2. Ventricular arrhythmias.

Arrhythmia vulnerability was evaluated as the number of ventricular arrhythmic events (VAEs) during the 15-minute baseline and stress periods. In all animals, VAEs mostly consisted of isolated premature beats and a few salvos (two or three consecutive premature beats; Fig. 4a).

Before GF/V injection, VAEs were negligible during baseline in all groups (Table 4). Stress exposure significantly increased VAEs in SO and MI groups but the increment was about two-fold higher in MI animals ($p<0.05$ vs. SO Fig. 4b). Two weeks after GF/V injection, baseline-VAEs remained unchanged in all groups (Table 4) while stress-induced VAEs were markedly reduced in MI+GF rats ($p< 0.02$) but not in SO+V and MI+V animals (Fig. 5). Thus, cytokine treatment lowered the proneness to arrhythmias triggered by stress-induced sympathetic stimulation in conscious animals with chronic myocardial infarction.

2 Ventricular mechanical performance.

2.1. Echocardiographic measurements.

Before GF/V injection, a global deterioration in cardiac anatomy and function was observed in the MI group when compared with the SO group (Table 5). Echocardiographic data measured in MI were characterized by: a) a significant reduction ($p<0.01$) in ejection fraction (EF: -8%) and fractional shortening (FS: -15 %), b) a significant increase ($p<0.01$) in left ventricular systolic diameter (LVSD: +36%), end-diastolic diameter (LVEDD: +15%), left ventricular end-systolic volume (LVESV: +188%), and left ventricular end-diastolic volume (LVEDV: +57%).

Two weeks after injection, in the MI+V animals, the morpho-functional properties of the left ventricle either remained unchanged or underwent a slight further deterioration (Fig. 6). In contrast, in the MI+GF rats, the treatment was followed by an improvement in LVEDD and LVEDV values, which approached those measured in the SO+V group (Fig. 6), suggesting a positive effect of GFs on left ventricular remodeling.

Moreover, in the MI+V group, infarct size (morphometrically determined, see below) was negatively correlated with fractional shortening and ejection fraction and positively correlated with LVSD and LVESV ($p<0.05$; Fig. 7 a-d). These correlations disappeared in MI+GF group (Fig. 7 a'-d') further supporting the hypothesis that the administration of HGF+IGF-1 induced a partial recovery of ventricular mechanical performance.

2.2 Hemodynamic measurements.

Invasive hemodynamic measurements were characterized by a substantial reduction in arterial blood pressure, systolic ventricular pressure and peak positive and negative ventricular dP/dt in MI+V and MI+GF groups when compared with SO+V (Fig. 8). However, the impairment of dP/dt and LVEDP was correlated with post mortem determination of infarct size in the MI+V group (Fig. 9 a-b) but not in the MI+GF group (Fig. 9 a'-b'). In line with echocardiographic data, these findings confirm that GF treatment abolishes the proportional deleterious effect of infarct size on the LV mechanical performance.

3 Ventricular electrical performance.

3.1 Epicardial multiple lead recording.

To minimize the invasiveness of the surgical procedure and ensure animal survival, all pre-GF/V injection measurements were obtained using the 5x5 electrode array (Fig. 3b). Instead, the post-GF/V-injection measurements, carried out before sacrifice, were performed using the 8x8 array (Fig. 3b) to allow for a wider exploration of the epicardial surface. Furthermore, the appropriate positioning on the ventricular epicardium of the array was in some cases prevented by an unfavorable spatial relationship between heart and lungs in the open chest preparation. Because of this and the presence of scattered fibrotic areas in the infarcted region, only a fraction of the 25-64 sites explored by epicardial electrodes were excitable and/or enabled the recording of reliable EG signals.

3.1.1 Excitability.

Globally, 121, 120 and 114 Strength-Duration (S-D) curves and as many Rheobase (Rh) and Chronaxie (Chr) values (Fig. 3f) were determined in the MI, MI+V and MI+GF groups respectively. Before injection, Rh and Chr in MI animals were 114±10 μA and 1.2±0.04 ms respectively. Cytokines shifted upward and to the right S-D curves and concurrently Rh and Chr values in MI+GF rats were slightly higher than those measured in MI+V group (Fig. 10a).

3.1.2. Conduction velocity.

Given the limited number of electrodes of the 5x5 array, no reliable conduction velocity (CV) measurements could be performed in the MI rats and only post-injection data were collected in the MI+V and MI+GF groups. CV was computed longitudinally (CV-l) and transversally (CV-t) to fiber orientation (Fig. 3e) at 114 and 112 epicardial sites in MI+V animals and 92 and 100 sites in MI+GF rats. The values of both CV-l and CV-t were similar in the two groups (Fig. 10b), suggesting that growth factor administration did not have any sizable effect on the spread of excitation at the epicardial surface.

3.1.3. Refractoriness.

The effective refractory period (ERP) was measured at 87, 113 and 92 epicardial sites in the MI, MI+V and MI+GF animals respectively. In the MI rats the average ERP value was 88.8±2.4 ms. After GF/V injection, ERP was about 30% longer in the MI+GF animals when compared with the MI+V group (Fig. 10c, $p<0.01$). A longer ERP would reduce the probability of reentry circuits provided that CV increases or remains constant *(van Rijen HV et al. 2006*). Thus, by the combined effect on conduction velocity and

refractoriness, cytokine treatment is expected to reduce cardiac electrical instability. Indeed, stress-induced VAEs were significantly reduced in GF treated animals.

3.1.4. ERP dispersion and QTc interval duration.

The degree of dispersion of ERP values and the duration of QTc interval were comparable in all animals (Fig. 10 d-e), suggesting that the influence of GFs on propensity to reentrant arrhythmias was not mediated by changes in the spatially non-uniform distribution of refractoriness. Furthermore, the longer ERP in MI+GF animals does not seem attributable to the longer duration of the recovery process.

4. Molecular analysis.

4.1. Electrophoretic and immunoblot analysis: Connexin43 expression.

Quantification of Cx43 expression was performed by western blot analysis on samples of the infarcted and remote portions of the rat hearts. The levels of Cx43 within the infarcted region were negligible in the MI+V group (Fig. 11) whereas local GF administration increased by about 10-fold ($p<0.01$) the expression of the gap junctional protein, suggesting a better electrical coupling within the scarred partially regenerated myocardium. Similar findings, although of lower magnitude (about 30% increase, $p<0.05$), were observed in the remote myocardium (Fig. 11).

4.2.Quantitative RT-PCR measurements of Ito current subunits.

To determine whether an altered modulation of transient outward K current (I_{to}) could affect ERP, the major isoforms of the rat alpha (Kv4.2, Kv4.3, Kv1.4) and beta (KChIP2) subunits were measured at mRNA level in the peri-infarcted and remote (left and right) ventricular myocardium of the MI+V and MI+GF rats, in comparison with SO+V. The mRNA expression for Kv4.2 and Kv4.3 alpha subunits in each myocardial region was similar in all animals. Conversely, Kv1.4 and the accessory subunit of the K channel KChIP2 were significantly increased by MI, in the remote left and right ventricular myocardium (Kv1.4: about +50%, $p<0.05$) (Fig. 12 a,c), and peri-infarcted and remote LV myocardium (KChIP2: about +100% and +20% , $p<0.01$) (Fig. 12b). In both cases, the rise was prevented by cytokines.

5. Cardiac Remodeling.

5.1. Cardiac Anatomy.

Compared with the SO+V animals, the MI+V group exhibited a significant increase in chamber volume associated with a moderate thinning of the left ventricular wall, resulting in a decreased mass-to-chamber volume ratio (Table 6). These markers of unfavorable remodeling, representing the major anatomical determinants of heart failure, were attenuated in the MI+GF rats (Table 6).

5.2. Morphometric Measurements.

Myocardial fibrosis and small foci of collagen accumulation, uniformly distributed throughout the LV wall, were detected in the spared non-infarcted ventricular myocardium of both MI+V and MI+GF groups. However, the volume fraction of interstitial fibrosis and the number of foci of replacement fibrosis were more than 2-fold lower in the treated MI+GF hearts ($p<0.01$; Fig. 13a-b).

5.3. Myocyte Cell Size.

The average cell size was larger in infarcted hearts as compared with the SO+V group. However, a statistically significant difference was reached only in the MI+V rats ($p<0.05$ vs. SO+V; Fig. 13c), indicating that reactive cellular hypertrophy was reduced by intramyocardial injection of GFs

5.4. Myocardial regeneration.

Areas of myocardial regeneration were detected in the infarcted portion of GF treated rat hearts. Small BrdU+ myocytes, expressing N-Cadherin (Fig. 14a) and Cx43 (Fig. 14b) were observed, indicating that newly formed, electromechanically coupled cardiac myocytes resulted from local injection of GFs. Within the two weeks from cytokine injection a nearly 3-fold increase in cycling myocytes accumulated in MI+GF infarcts when compared with the MI+V ones (Fig. 14c). The formation of electromechanically competent myocytes was also present in the peri-infarcted and remote myocardium of treated animals, suggesting that local delivery of growth factors exerted a global beneficial effect on the heart (Fig. 14c). Although similar findings could occasionally be detected in untreated chronic infarcts, the quantitative estimation clearly indicated that the regenerative processes were markedly enhanced in the MI+GF

group in both the peri-infarcted and infarcted areas (Fig. 14c). Importantly, the newly formed myocardium was properly perfused, as indicated by the significant increase in the density of arteriolar profiles (two-fold) and $BrdU^+$ endothelial cells (five-fold) (Fig. 14 d-f).

Infarct size was similar in the two experimental groups in which the average values of lost myocytes was approximately equal to 4.5×10^6. Within the infarcted area, cytokine treatment promoted the formation of an average of $5.9 \pm 0.1 \times 10^6$ developing myocytes ranging in size from 200 to a maximum of 4000 μm^3 (Fig. 15a). Most newly formed cardiomyocytes had a volume of less than 2000 μm^3, although cytokine treatment was able to generate a consistent number of cells approaching a volume of 4000 μm^3. Conversely, myocardial repair in untreated infarcts was unremarkable. The generation of new myocytes increased linearly with the amount of cell loss in GF treated animals. A similar reparative capacity was not observed in untreated rats (Fig. 15b). The observation that myocardial regeneration was associated with intense activation and translocation of resident progenitor cells (Fig. 15c) strongly suggested that GF-induced cardiac repair was mediated by a multipotent stem cell population. Indeed, in comparison with MI+V, a significant ($p<0.01$) increase in the incidence of c-kit^+ cells was produced by GFs in the infarcted, peri-infarcted and remote myocardium (Fig. 15c).

Figures and Tables of protocol A

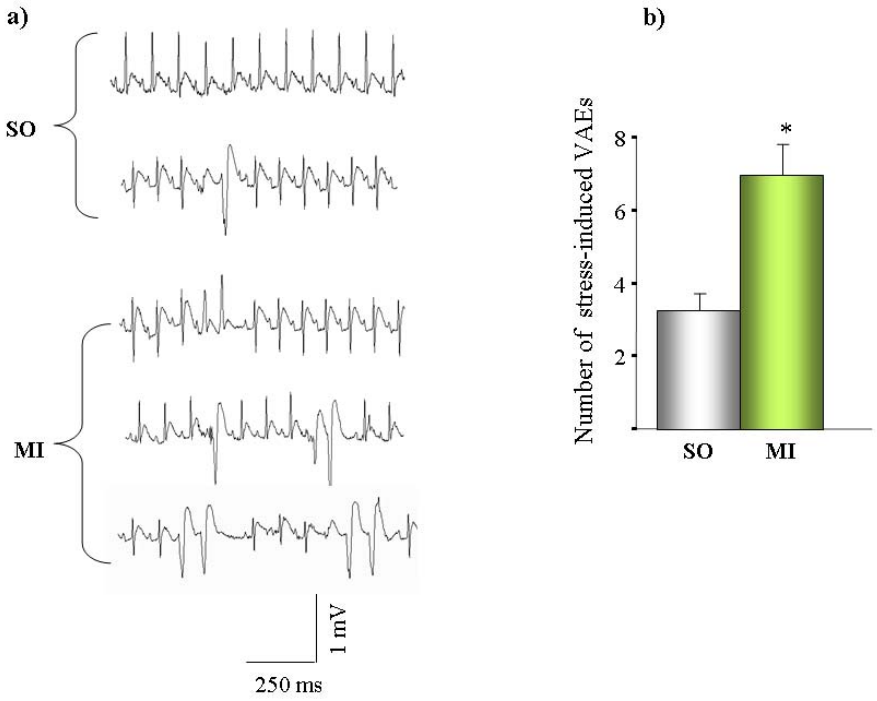

Fig. 4. Ventricular arrhythmic events.
a) Telemetry-ECG recordings during social stress from representative SO (upper tracings) and MI animals (lower tracings) showing the different types and severity of ventricular arrhythmic events (VAEs).
b) Average values ± SE of the number of VAEs occurring in SO and MI groups, during stress exposure.
* $p<0.01$ vs. SO.

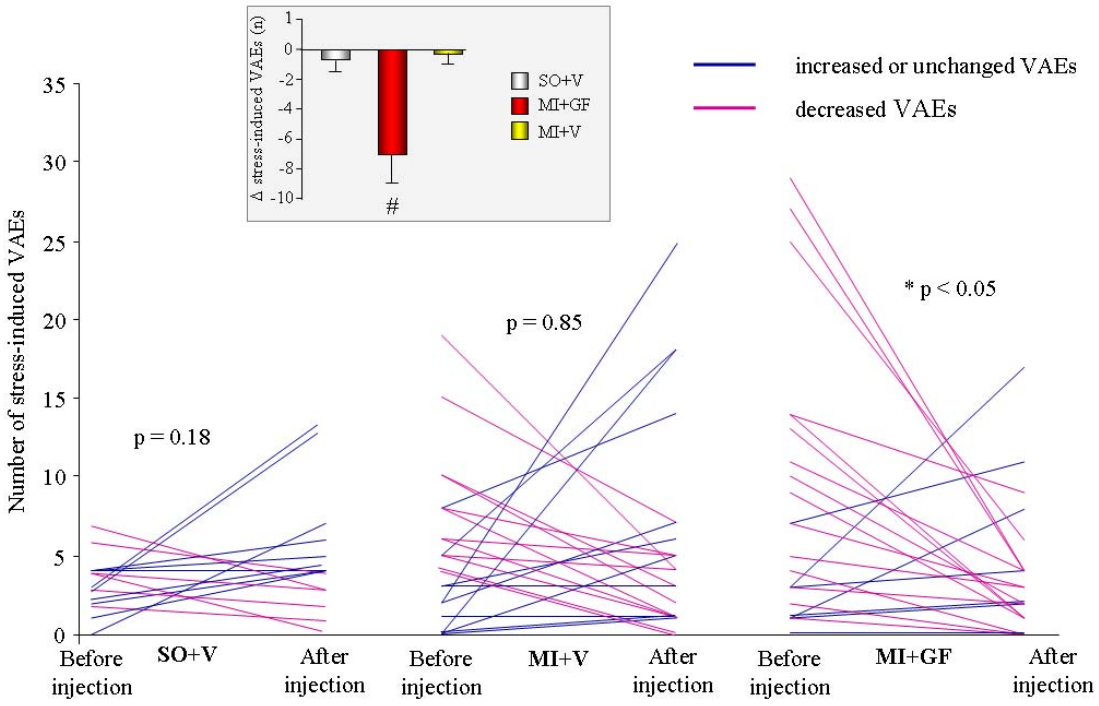

Fig. 5. Effects of GF/V injection on the proneness to stress-induced arrhythmias
Changes in the number of stress-induced VAEs after GF/V injection, in each animal of SO+V, MI+V and MI+GF groups. * $p<0.02$ vs. pre-injection values, within MI+GF group. The insert shows the average values±SE of the difference (Δ) between the number of VAEs measured before and after GF/V injection, in each experimental group. # $p<0.01$ vs. SO+V and MI+V.

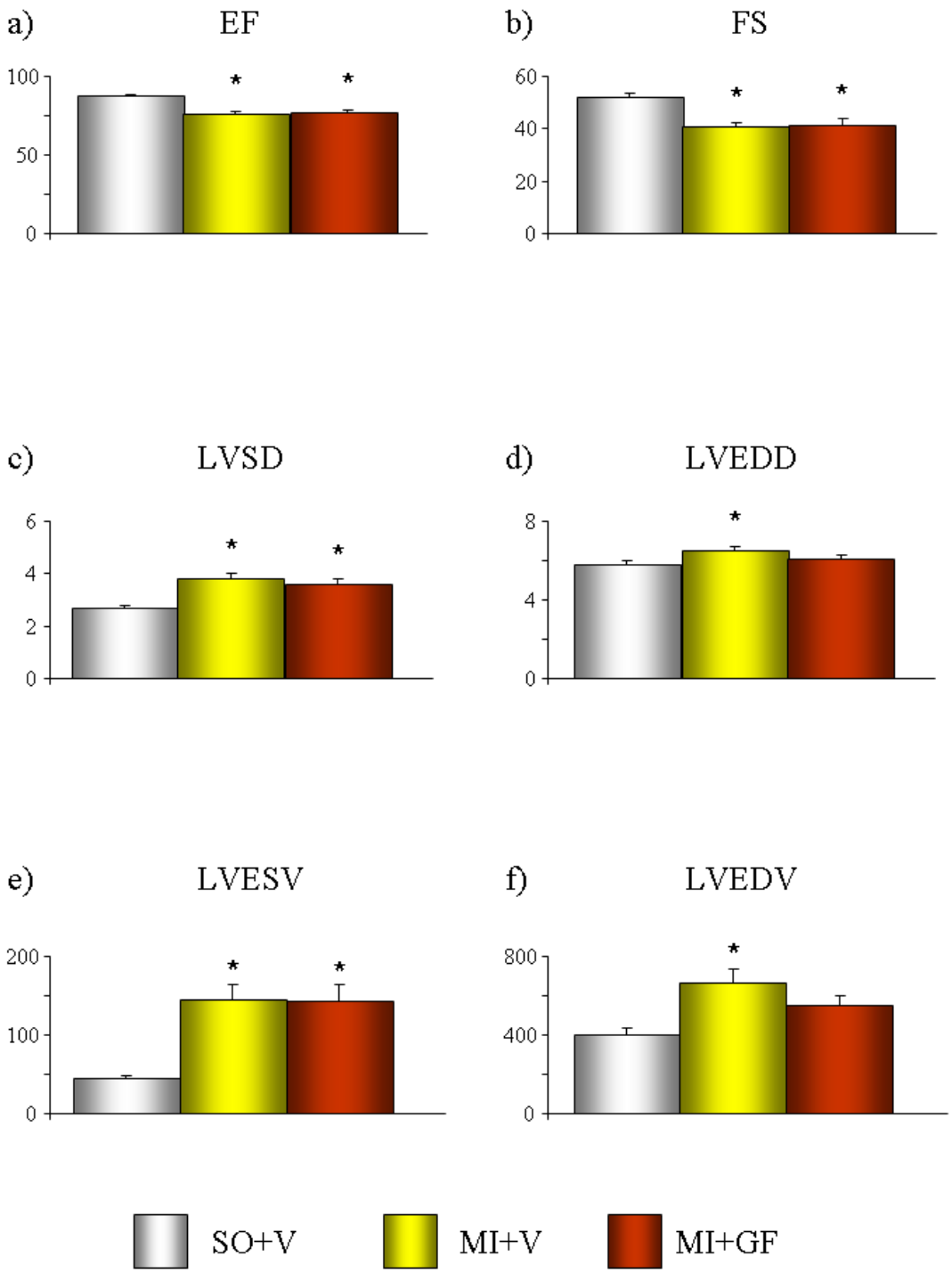

Fig. 6. Post-injection echocardiographic measurements
Mean values ± SE of a) EF, b) FS, c) LVSD; d) LVEDD, e) LVESV and f) LVEDV measured 15 days after treatment in SO+V, MI+V and MI+GF groups.
*p<0.01 significant differences between SO+V.

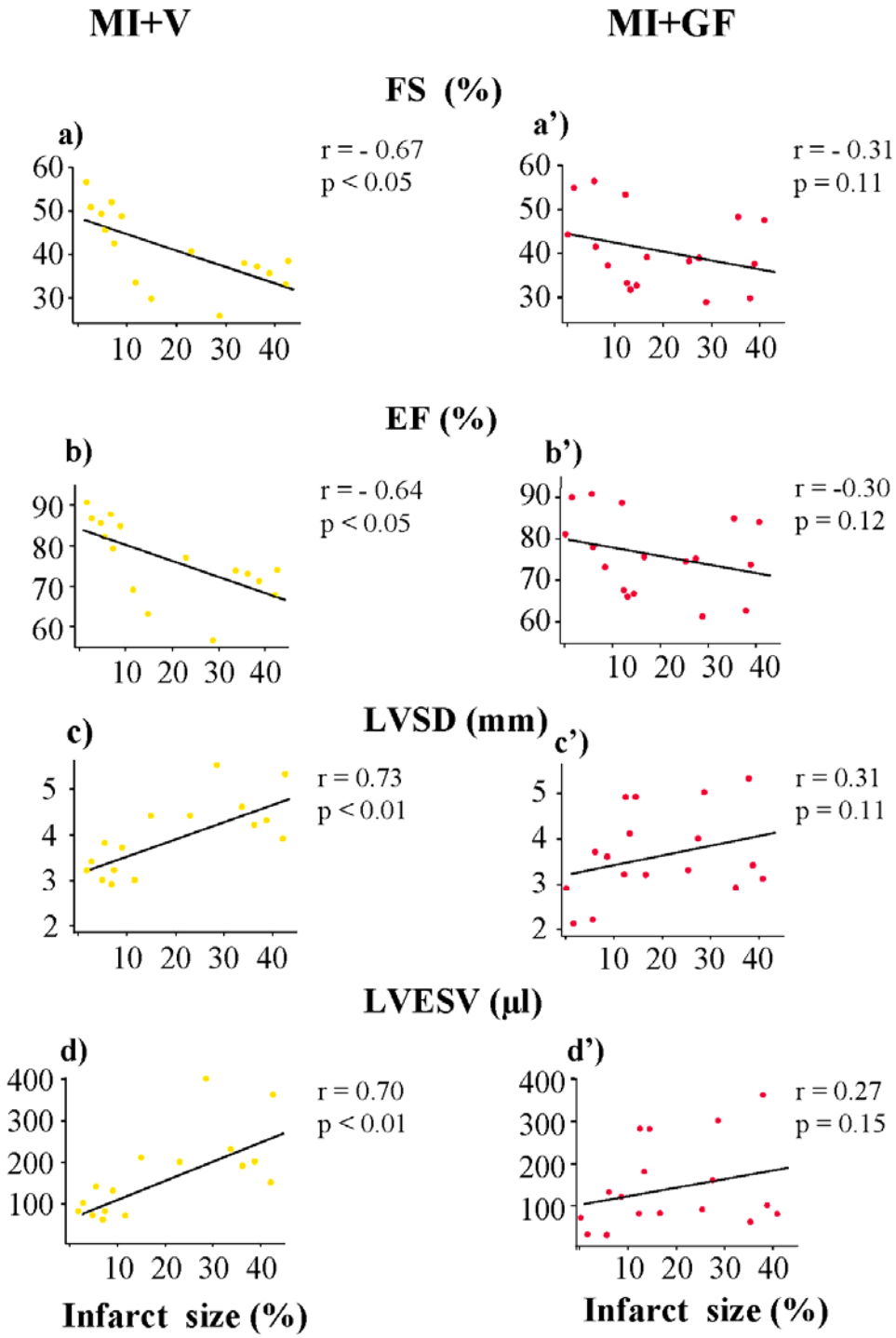

Fig. 7. Blunting effect of GF treatment on the correlation between infarct size and echocardiographic parameters

Linear correlations between infarct size and fractional shortening (FS), ejection fraction (EF), left ventricular systolic diameter (LVSD) and left ventricular end-systolic volume (LVESV), in MI+V (a-d) and MI+GF (a'-d') animals.

The statistical significance of correlations was limited to the MI+V group.

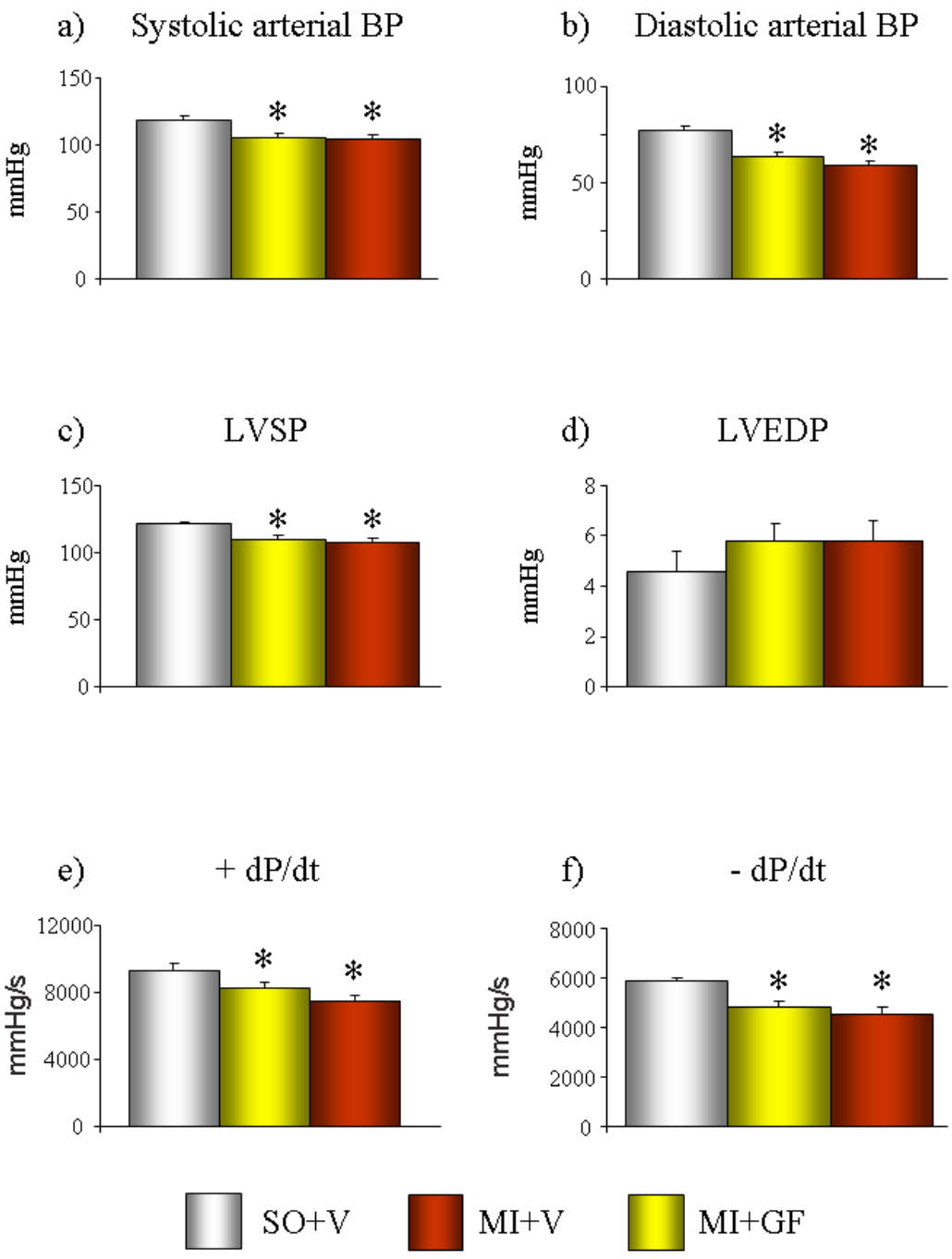

Fig. 8. Hemodynamic measurements
Mean values ± SE of a) Systolic arterial blood pressure (BP), b) Diastolic arterial BP, c) LVSP, d) LVEDP, e) + dP/dt and f) - dP/dt, in SO+V, MI+V and MI+GF animals.
* $p < 0.01$ significant differences vs. SO+V.

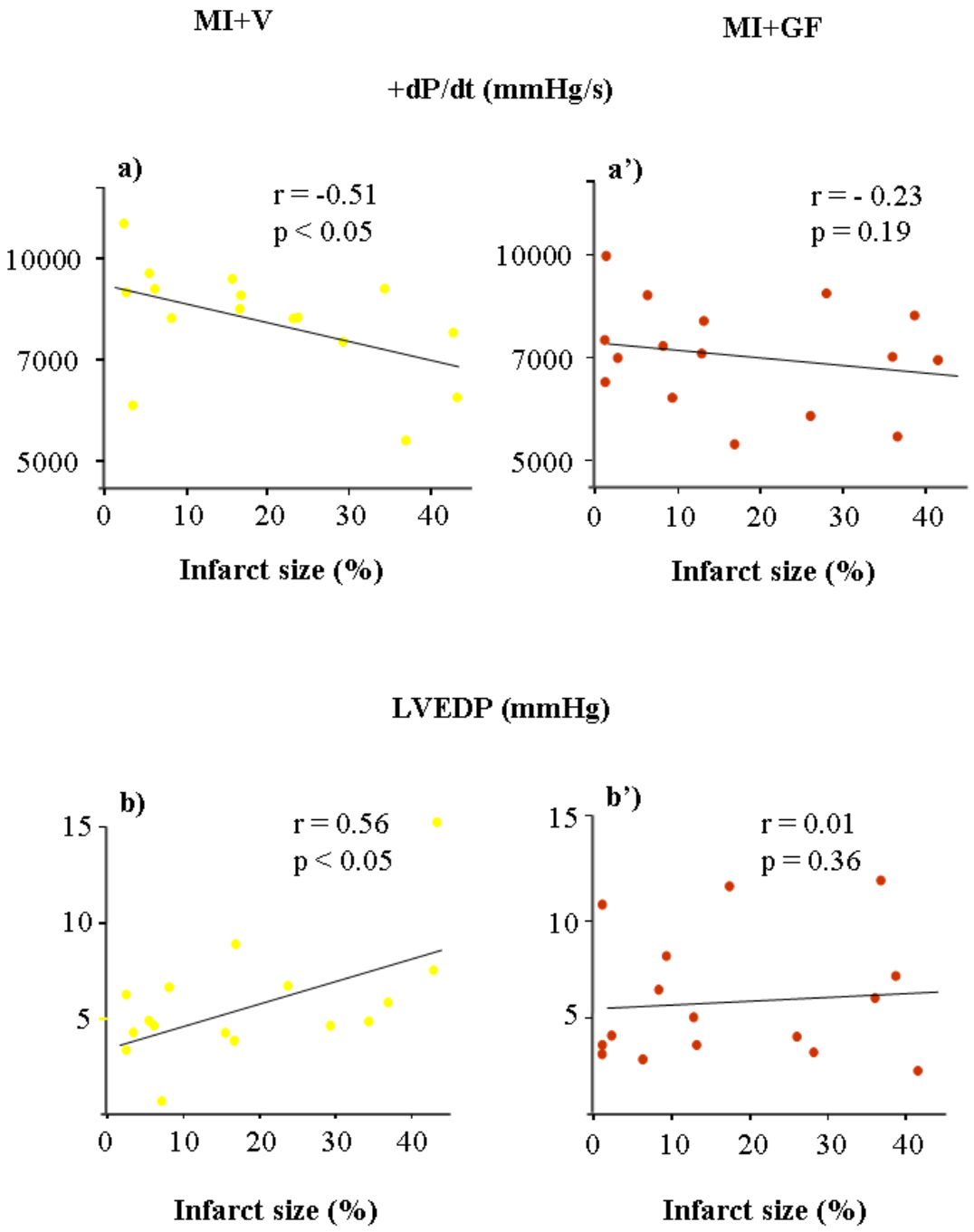

Fig. 9. Blunting effect of GF treatment on the correlation between infarct size and hemodynamic parameters

Linear correlations between infarct size and maximum rate of ventricular pressure rise (+dP/dt) and left ventricular end-diastolic pressure (LVEDP), in MI+V (a-b) and MI+GF animals (a'-b').

The statistical significance of correlations was limited to the MI+V group.

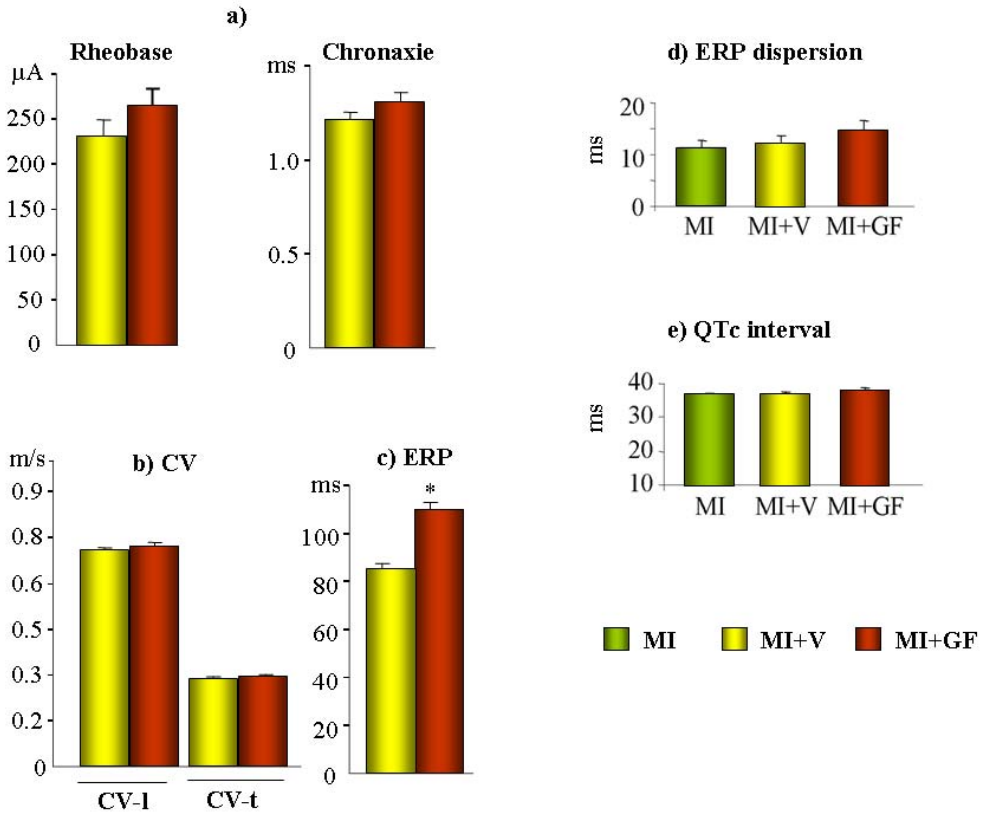

Fig. 10. Epicardial multiple-lead recording
The bar graphs illustrate the mean values±SE of: (a) rheobase and chronaxie, (b) conduction velocity along (CV-l) and across (CV-t) epicardial fiber direction, (c) effective refractory period (ERP), (d) ERP dispersion and (e) QTc interval duration in MI (before GF/V injection), MI+V and MI+GF groups (after GF/V injection).
* $p<0.05$ vs. MI+V.

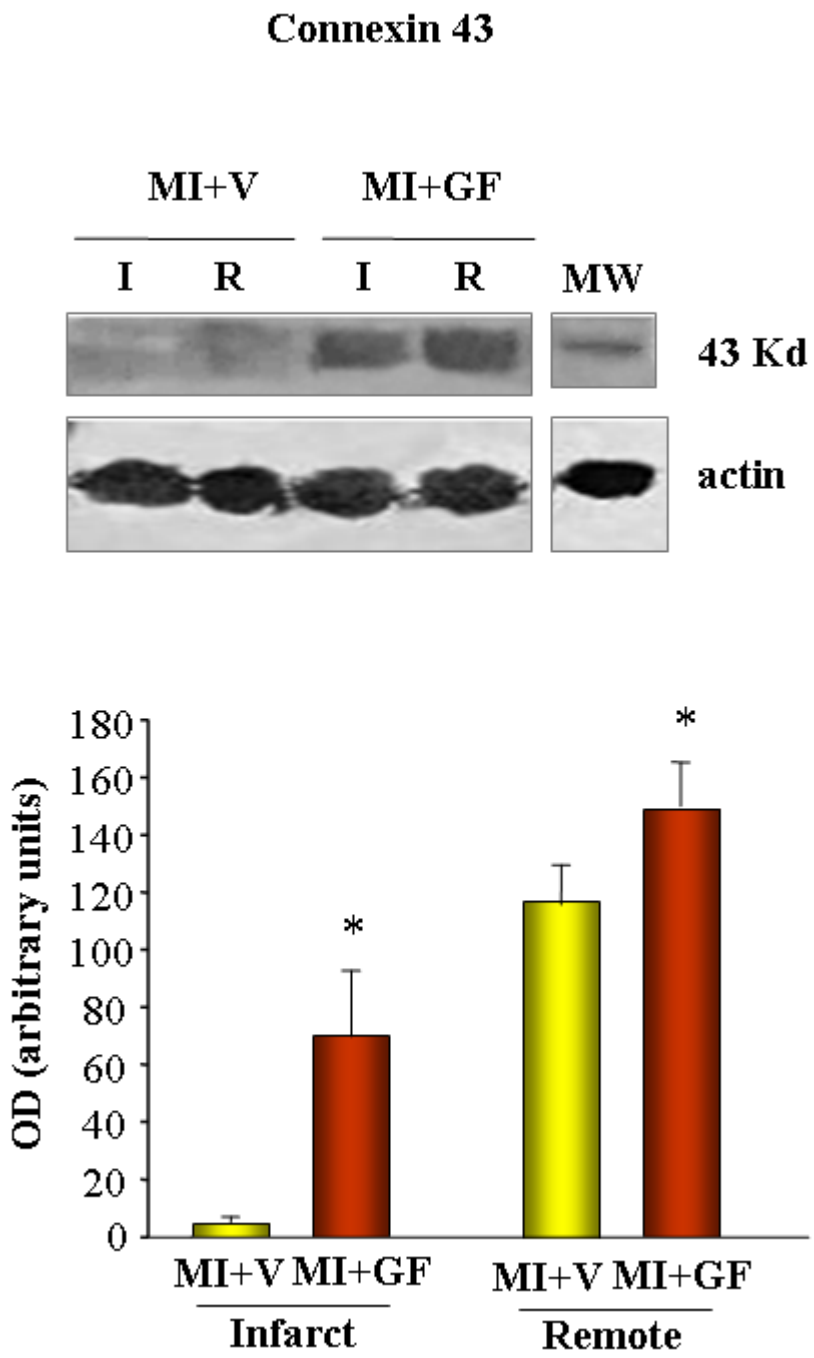

Fig. 11. Quantification of connexin43 protein expression.
Western blot analysis of connexin43 protein expression in infarcted (I) and remote (R) left ventricular myocardium of MI+V and MI+GF hearts. MW=molecular weight marker; OD=optical density.
* $p<0.05$ vs. MI+V.

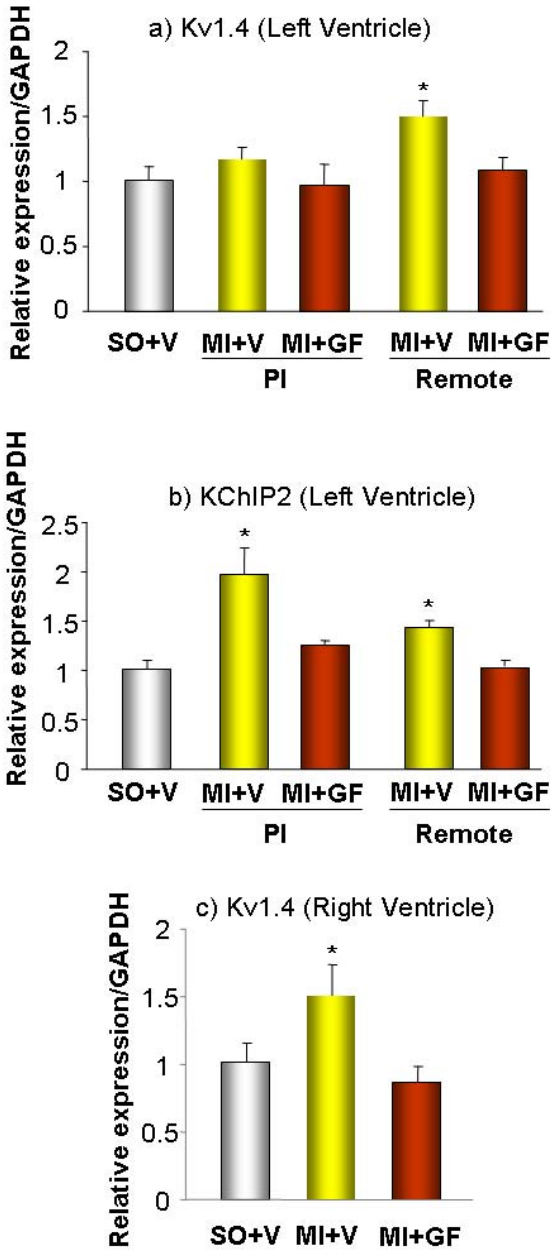

Fig. 12. Expression of K channel isoforms
Quantification of Kv1.4 (a, c) and KChIP2 (b) m-RNA levels, in ventricular myocardium. PI: peri-infarcted; Remote: spared left ventricular myocardium. Each bar represents the mean of 4 different samples in triplicate.
* $p<0.05$ vs. SO+V and MI+GF.

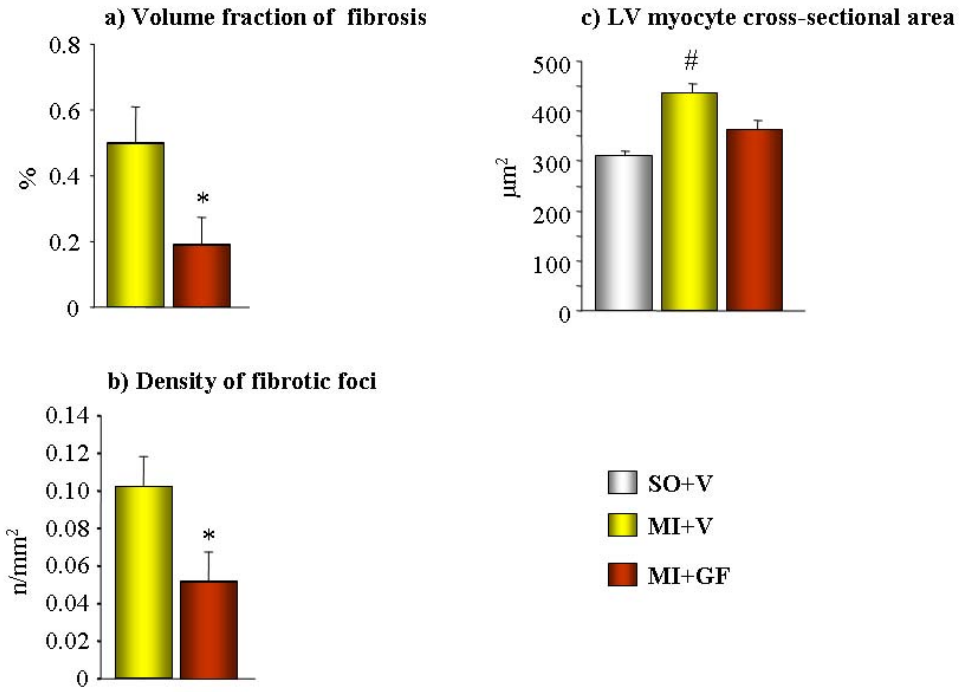

Fig. 13. Myocardial fibrosis and left ventricular myocyte size
Mean values±SE of volume fraction of fibrosis (a), and numerical density of fibrotic foci (b), morphometrically evaluated in the remote left ventricular (LV) myocardium of MI+V and MI+GF hearts. In (c), mean values±SE of the LV myocyte cross-sectional area.
* $p<0.05$ vs. MI+GV;
# $p<0.05$ vs. SO+V.

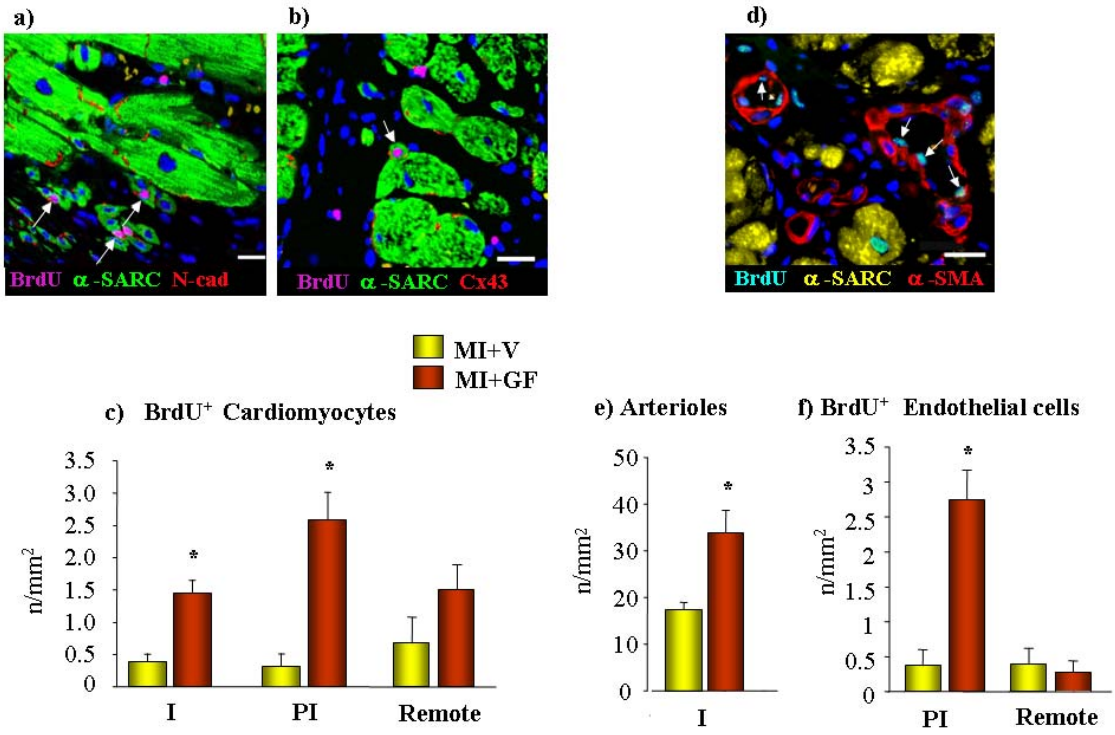

Fig. 14. Myocyte and Vessel Regeneration
Immunofluorescence staining of sections of the infarcted (a,b,d) myocardium of GF treated rats. Arrowheads indicate BrdU labeled (a-b, pink fluorescence) nuclei of small α-sarcomeric actin positive cardiomyocytes (α-SARC, green fluorescence) showing in red fluorescence mechanical (a, N-cad=Ncadherin) and electrical (b, Cx43=connexin43) connections. Blue fluorescence corresponds to DAPI labeling of nuclei. Scale Bars: a) 20μm; b) and d) 50μm. Bar graphs illustrate the quantification of proliferating cardiomyocytes (c) in the infarcted (I), peri-infarcted (PI) and remote myocardium of vehicle (V) and Growth Factor (GF) treated hearts. * $p<0.05$ vs. MI+V.
Bar graphs illustrate the quantification of (e) the absolute number of arterioles in the infarcted (I) myocardium, and of (f) endothelial cells in the peri-infarcted (PI) and remote myocardium of vehicle (V) and Growth Factor (GF) treated hearts.
* $p<0.05$ vs. MI+V.

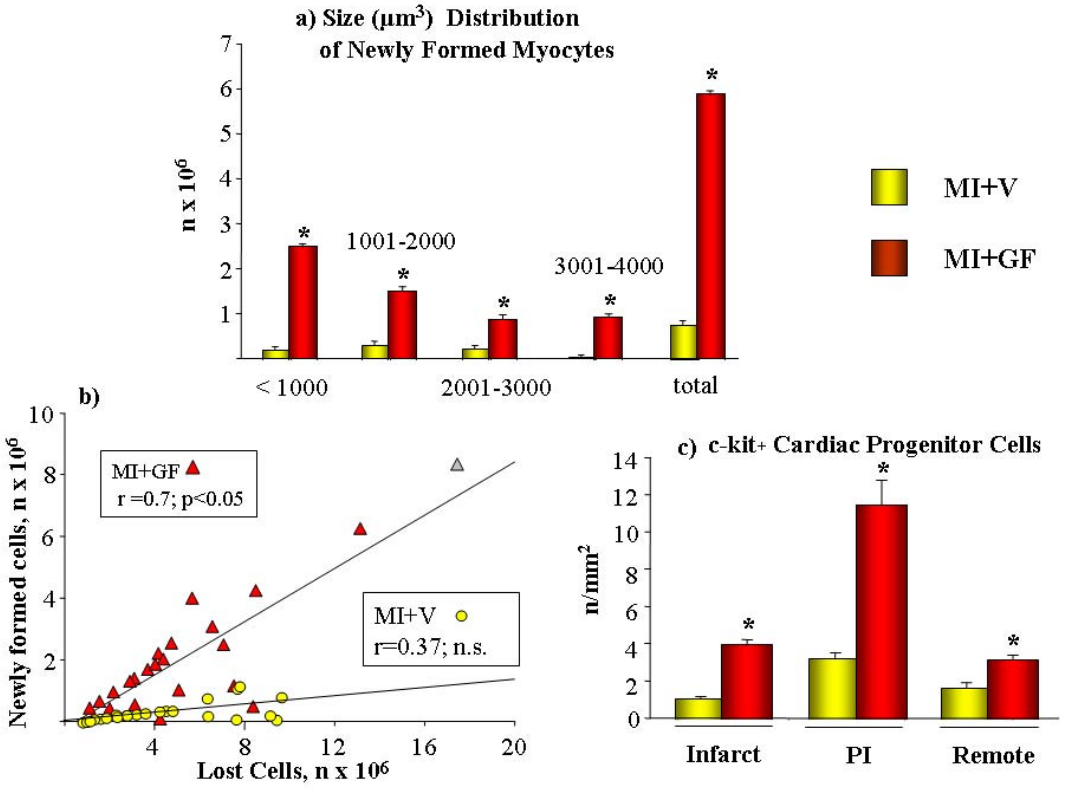

Fig. 15. Quantitative analysis of cardiomyocyte loss and regeneration, and progenitor cell mobilization

a) Size distribution of newly formed cardiomyocytes in the infarcted area; b) correlation between number of lost cells and newly formed myocytes; c) density of c-kit+ cardiac progenitors in the infarcted, peri-infarcted (PI) and remote myocardium.

In bar graphs data are reported as mean values±SE for treated and untreated MI animals.

Table 3. Mean values ± SE of R-R interval, and R-R interval variability indices (SD_{RR} and r-MSSD) measured in baseline and stress conditions in the various experimental groups, before and after GF/V injection.

	Before GF/V injection		**After GF/V injection**		
	SO (n=15)	**MI (n=45)**	**SO+V (n=15)**	**MI+V (n=23)**	**MI+GF (n=22)**
R-R interval (ms)					
baseline	170 ± 5.3	172 ± 3.5	182±.5.8	167 ± 4.8 #	183 ±4.8
social stress	123 ± 2.9 **§**	120 ± 1.0 **§**	123 ±.2.4 **§**	122 ±1.2 **§**	125 ±1.8 **§**
SD_{RR} (ms)					
baseline	11.0 ± 0.4	10.7 ± 0.6	10.3 ± 0.7	9.9 ± 0.5	11.7 ± 0.7
social stress	7.2 ± 0.8 **§**	5.7 ± 0.4 **§**	6.4 ± 0.9 **§**	5.2 ± 0.4 **§**	6.5 ± 0.7 **§**
r-MSSD (ms)					
baseline	3.7 ± 0.3	4.9 ± 0.3	4.0 ± 0.4	4.3 ± 0.3	5.0 ± 0.4
social stress	2.7 ± 0.2 **§**	3.0 ± 0.l **§**	2.9 ± 0.3 **§**	3.3 ± 0.2 **§**	3.3 ± 03 **§**

§ $p<0.01$ significant differences vs. baseline, within each group; # $p<0.05$ significant differences vs. SO+V and MI+GF.

Table 4. Ventricular arrhythmic events during baseline

	Before GF/V injection		After GF/V injection		
Groups (number of animals)	**SO** (15)	**MI** (45)	**SO+V** (15)	**MI+V** (23)	**MI+GF** (22)
PVBs (range)	(0-1) in 1 rat	(1-6) in 5 rats	none	(1-2) in 4 rats	(1-19) in 5 rats
Salvos (range)	none	(0-1) in one rat	none	none	none
number of animals without arrhythmias	14 out of 15	39 out of 45	all rats	19 out of 23	17 out of 22

PVBs: premature ventricular beats; Salvos: 2-3 consecutive premature ventricular beats.

Table 5. Pre-injection echocardiographic measurements

	Pre-injection	
	SO (n=9)	**MI (n=38)**
EF (%)	89.5±0.9	82.4±1.2 *
FS (%)	54.8±1.4	46.8±1.2 *
LVSD (mm)	2.5±0.1	3.4±0.1 *
LVEDD (mm)	5.5±0.2	6.3±0.2 *
LVESV (µL)	42±8	121±5 *
LVEDV (µL)	397±43	625±44 *

Mean values±SE of echocardiographic parameters measured before GF/V injection in SO and MI groups.
EF: ejection fraction; FS: fractional shortening; LVSD: left ventricular systolic diameter; LVEDD: left ventricular end-diastolic diameter; LVESV: left ventricular end-systolic volume; LVEDV: left ventricular end-diastolic volume.
*$p<0.01$ significant differences between SO and MI

Table 6. Mean values ± SE of left ventricular (LV) geometrical properties measured in SO+V, MI+V and MI+GF groups.

	SO+V (n=15)	**MI+V (n=17)**	**MI+GF (n=21)**
LV mass (mm^3)	769 ± 43	1046 ± 35 *	1031 ± 17 *
LV wall thickness (mm)	2.2 ± 0.1	2.0 ±0.1	2.2 ± 0.1
LV chamber diameter (mm)	5.5 ± 0.2	7.2 ± 0.2 *	6.7 ± 0.2 *
LV chamber volume (mm^3)	199 ± 11	413 ± 25 *	336 ± 18 * #
mass/chamber volume	4.1 ± 0.1	2.4 ± 0.1 *	2.9 ± 0.2 *
Infarct size (%)	__	19.4 ± 3.2	19.9 ± 2.9

* $p < 0.01$ significant differences vs. SO group; # $p < 0.05$ significant differences between MI+V and MI+GF.

Results of protocol B

Telemetry-ECG recording

Hear rate and R-R interval variability (SD_{RR} and r-MSSD.)

During baseline, the average values of heart rate and heart rate variability indexes did not show any significant differences among groups (average values: heart rate approximately 350 bpm, SD_{RR} 11.4 ms and r-MSSD 5.4 ms). As expected, in all groups the exposure to social stress significantly increased heart rate (+ 39%, on average) and reduced SD_{RR} (-45%) and r-MSSD (-43%). Thus, intramyocardial delivery of HMGB1 protein as well as its inactive form did not markedly affect heart rate and the autonomic modulation of heart rate (Fig. 16).

Cardiac arrhythmias.

Arrhythmia vulnerability was evaluated as the number of ventricular arrhythmic events (VAEs) during the 15-min baseline and stress periods.

In comparison with SO, MI+boxA rats showed a significantly higher number of VAEs during both baseline and stress conditions ($p<0.01$; Fig.17). The increased proneness to arrhythmias was completely abolished in HMGB1-treated MI animals (Fig. 17), suggesting a protective effect of protein injection against spontaneous arrhythmias as well as arrhythmias triggered by sympathetic stimulation.

Figures and Tables of protocol B

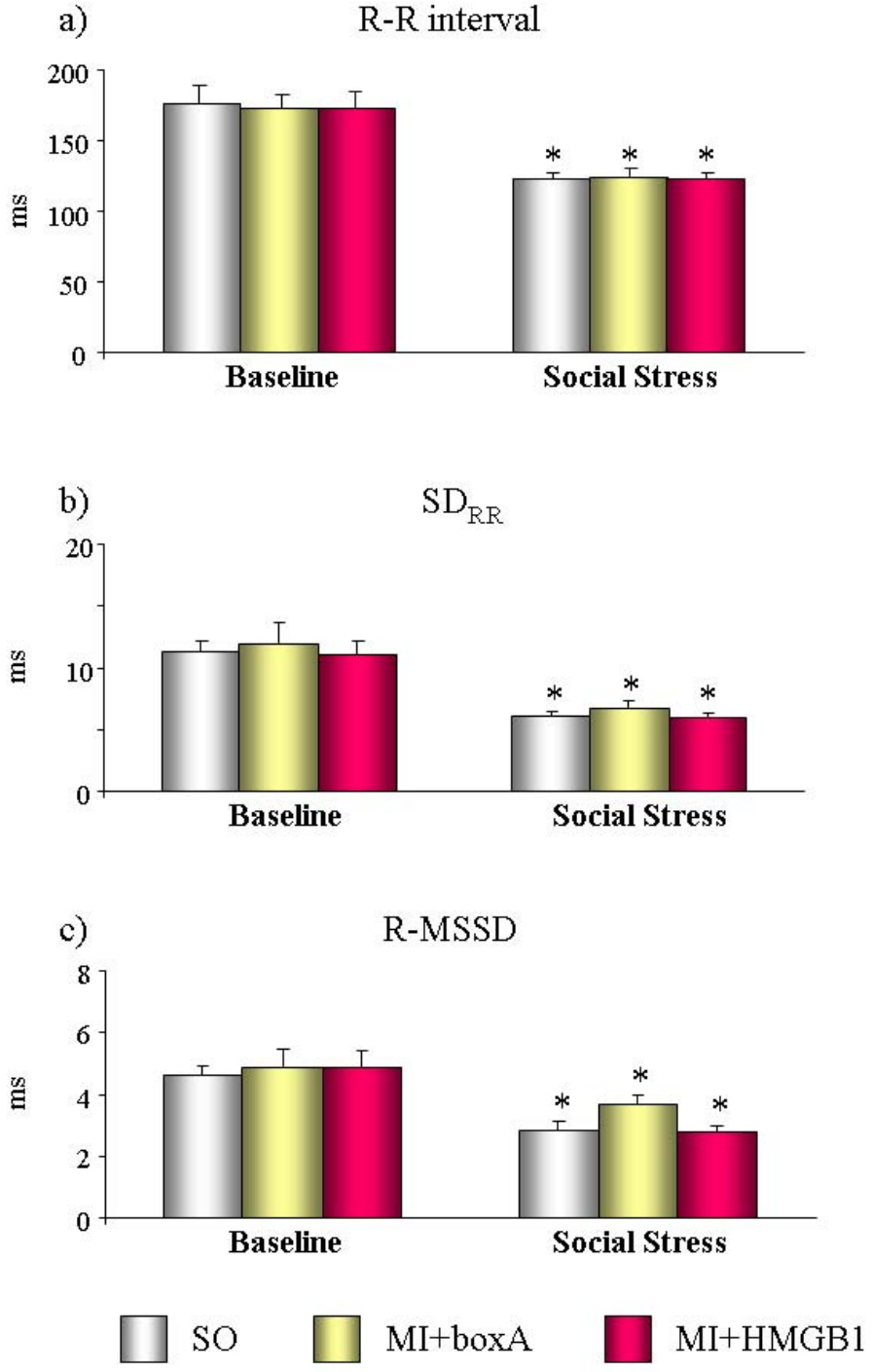

Fig. 16. R-R interval and R-R interval variability (SD_{RR} and r-MSSD)
Average values ± SE of (a) R-R interval, (b) SD_{RR} and (c) r-MSSD during baseline and social stress periods ,in the different experimental groups.
* Significant differences between baseline recording periods within each group.

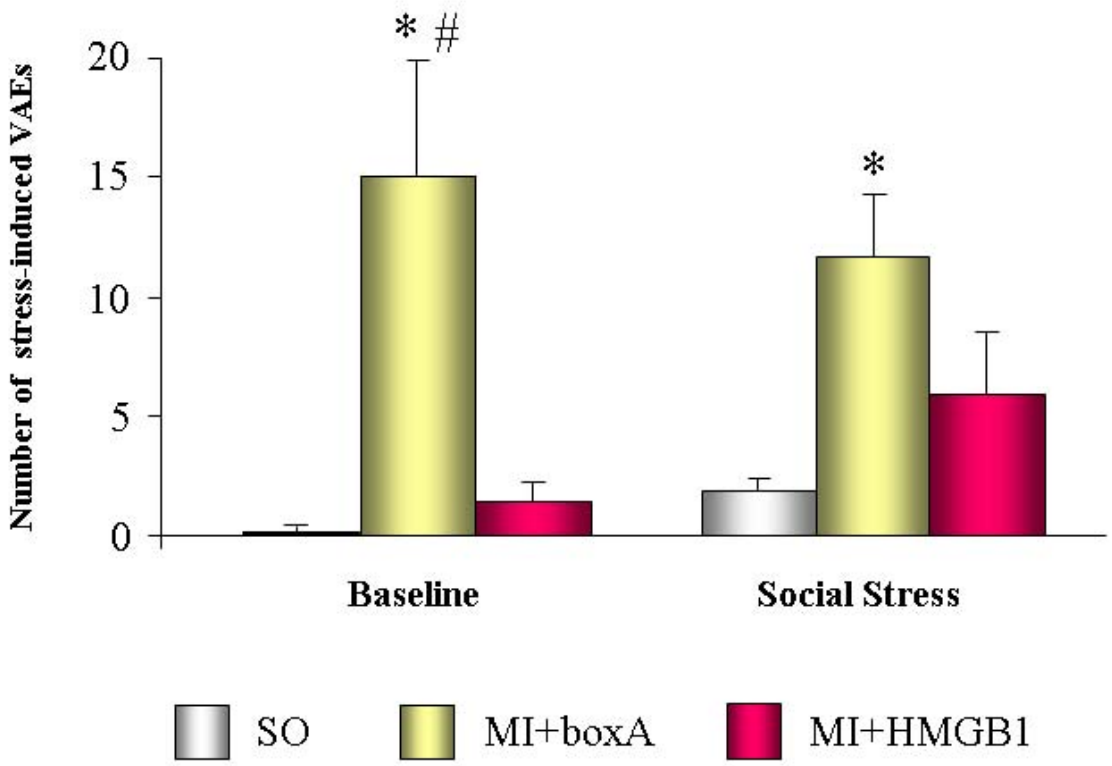

Fig. 17. Ventricular arrhythmic events
Average values ± SE of the number of ventricular arrhythmic events (VAEs) during baseline and social stress periods, in each experimental group
* $p<0.05$ vs.SO
# $p<0.05$ vs.MI+HMGB1

Discussion

During the last decade, a growing number of experimental and clinical observations have shown that therapies based on the mobilization/injection of stem cells of different origins can ameliorate the mechanical function and perfusion of the ischemic heart (*Dimmeler S et al. 2005; Leri A et al. 2005*). On the other hand, the induction or exacerbation of arrhythmias remains a major concern in stem cell based therapies for cardiac repair, and the effect of regenerative treatments on cardiac electrogenesis is still under debate (*Chen HS et al. 2009; Ly HQ et al. 2009; Macia E et al. 2009; Smith RR et al. 2008)*. The present research work specifically addressed this issue, in rat models with chronic or acute myocardial infarction.

Globally, data reported here support the hypothesis that mobilization of cardiac progenitor cells (CPCs) via intra-myocardial delivery of either GFs (HGF+IGF-1, chronic MI) or HMGB1 protein (acute MI), a mediator of the inflammatory response, leads to a significant decline in proneness to ventricular arrhythmias.

The results of the two experimental studies will be separately discussed.

A) STUDY ON CHRONIC MYOCARDIAL INFARCTION

Our results demonstrate that intra-myocardial injection of HGF and IGF-1 in a rat model of healed myocardial infarction caused a significant decline in proneness to ventricular arrhythmias, recorded in conscious freely moving animals subjected to stressful conditions. A potential underlying mechanism involved in this protective effect is the prolongation of the effective refractory period (ERP) at the epicardial surface of the regenerated heart, in the absence of changes in dispersion of refractoriness and duration of ventricular repolarization, as suggested by measurements of QTc interval and mRNA levels for K-channel α-subunits Kv4.2 and Kv4.3. Furthermore, markers of cardiomyocyte reactive hypertrophy, including mRNA levels for K-channel α-subunit Kv1.4 and β-subunit KChIP2, interstitial fibrosis and negative structural remodeling were significantly reduced in peri-infarcted/remote ventricular myocardium of GF-treated animals.

In support of previous data (*Linke A et al. 2005, Urbanek K et al. 2005; Rota M et al. 2008*), we also found that resident CPCs, stimulated locally by GF treatment, invaded the scarred myocardium and generated new electromechanically-connected myocytes and vessels. Experimental evidence was provided for a partial recovery of mechanical competence in the regenerated heart associated with an attenuation of unfavorable structural remodeling which involved the peri-infarcted and remote myocardium, suggesting that local delivery of GFs also exerted beneficial effects in the spared tissue.

Recovery of Electrical Function

Experimental studies aimed at assessing the proarrhytmic/antiarrhythmic potential of stem cell based therapies in vivo have been carried out mostly in anesthetized animals and in few cases in conscious animals during baseline conditions (*Kolettis TM 2006).* However, anesthesia can have confounding effects and the incidence of arrhythmias in baseline conditions is generally low. To circumvent these limitations, the proneness to arrhythmias was evaluated in conscious freely moving rats subjected to the resident-intruder test (*Martinez M et al. 1998*) which mimics stressful conditions encountered by social animals in every day life. The procedure is known to consistently induce an intense activation of the autonomic nervous system, with a shift of the sympatho-vagal balance towards a sympathetic predominance, resulting in arrhythmias even in normal animals (*Stilli D et al. 2004*). Stress-induced ventricular arrhythmias were reduced by about half following GF injection while no changes were observed in untreated rats, indicating a protective effect of local delivery of cytokines.

It has been recently reported *(Ly HQ et al. 2009*) that important issues to consider when assessing the effect of stem cell based myocardial regeneration on cardiac electrical competence include: (i) intrinsic electrophysiological properties of stem cells, (ii) modulated graft-host and/or graft-graft electromechanical coupling, (iii) changes in ion channel function, (iv) induced heterogeneity, and (v) altered myocardial tissue architecture comprising heterogeneous sympathetic nerve sprouting. All these factors may affect cardiac electrogenesis either by acting alone or in concert with the arrhythmic substrate of the injured myocardium.

We found that dispersion of refractoriness was similar in treated and untreated animals, as were the indirect indexes of autonomic input to the heart (SD_{RR} and r-

MSSD), suggesting that GFs did not alleviate arrhythmia susceptibility by affecting repolarization heterogeneity (*Fukushima S et al. 2007*) or cardiac sympathetic activity (*Pak HN et al. 2003*).

Quantitative RT-PCR analysis of the genes encoding the Ca^{2+}-independent transient outward potassium current (I_{to}), revealed that transcript expression of Kv1.4 was up-regulated in remote left ventricle only in untreated rats. Kv1.4 is the main channel subunit contributing to I_{to} during embryonic development of mouse and rat. After birth, Kv1.4 expression levels decrease, while Kv4.2 and Kv4.3 are up-regulated (*van der Heyden MA et al. 2006*). Importantly, cardiac hypertrophy induces a re-expression of Kv1.4 mRNA (*Marionneau C et al. 2008*). Further, the rise in mRNA levels of potassium channel β-subunit KChIP2 produced by myocardial infarction was abolished by GF administration. Recent studies documented higher mRNA levels of KChIP2 in cardiac hypertrophy (*Tozakidou M et al. 2010*) although a full appreciation of this result is impossible, since to date the role of KChip(s) subunit(s) has not been clearly elucidated. In conclusion, the lower mRNA levels of Kv1.4 and KChIP2 subunits produced by GF injection might be associated with the reduced reactive cellular hypertrophy following cardiac repair. These findings, together with anatomical and morphometric data, indicate that GF treatment may succeed in partially controlling endogenous arrhythmic substrates by limiting the unfavorable LV remodeling, and reducing myocardial fibrosis and reactive cellular hypertrophy in the remote myocardium, thereby contributing to prevent the occurrence of re-entry circuits.

By using epicardial multiple-lead recording, we showed that cytokine injection resulted in a marked prolongation of ERP, while conduction velocity (CV) was unchanged. The combined effect of CV and ERP on impulse propagation is defined by the wavelength L = CV x ERP, implying that a longer L (by increasing CV and/or

ERP) will reduce the likelihood that a single or multiple reentrant circuits can be accommodated by the heart (*van Rijen HV et al. 2006*). Hence, ERP changes observed in GF treated rats could reduce the ability of cardiac tissue to elicit an abnormal propagated response by increasing L, thus hampering reentry. The finding that epicardial QTc values were similar in all animals indicates that mechanisms other than lengthening of action potential duration (APD) were responsible for the longer ERP in GF treated rats. Accordingly, either membrane currents affecting APD were not influenced by GFs or, if they were, the net modification might not be large enough to manifest itself at the tissue level. Indeed, our data show that mRNA levels of the potassium channel α-subunits Kv4.2 and Kv4.3 did not exhibit any significant difference between untreated and HGF+IGF-1 treated hearts, suggesting that the transient outward potassium current (I_{to}), which contributes conspicuously to determine APD, was unaltered.

On the other hand, recent studies have demonstrated that IGF-1, alone or in combination with other growth factors, increases Cx43 expression in cardiac myocytes (*Hahn JY et al. 2008*). In support of these findings, we showed that GF administration significantly increased the expression of the gap-junctional protein Cx43, providing evidence for an increased electrical coupling within the scarred, partially regenerated myocardium as well as in the remote spared tissue. A better intercellular electrical connection is considered as being an important antiarrhythmic factor (*Hahn JY et al. 2008; Kuhlmann MT et al. 2006; Mills WR et al. 2007; Roell W et al. 2007; Duffy HS 2008; Gepstein L et al. 2010; Wang D et al. 2010*) and could also result in ERP prolongation. It has been remarked (*Fozzard HA 2001*) that the amount of current needed for cardiac excitation by point stimulation is modulated by the properties of

electrical coupling of the interconnected myocytes via gap-junctions. The smallest myocardial region capable of initiating a propagated action potential ("liminal length") is inversely related to the extra- and intracellular resistivities**,** which are largely dependent on interstitial fibrosis and electrical coupling between myocytes respectively (*Fozzard HA et al. 1972; Fozzard HA 2001*).

The role of myocardial geometry in the charge threshold for excitation was documented by computing the S-D curve, which shifted to the right when the "liminal length" increased (i.e. reduced excitability) and to the left when it decreased (i.e. increased excitability) (*Fozzard HA et al. 1972)*. Changes in "liminal length" resulting from different degrees of electrical coupling between myocytes are also expected to affect cardiac refractoriness, which will be increased by an increase in "liminal length" and reduced by its reduction. Concurrently, the longer ERP and the associated tendential shift to the right of the S-D curve induced by HGF+IGF-1 administration might be attributed to the higher expression of Cx43 and the longer "liminal length" resulting from an enhanced cardiomyocyte interconnection.

Cardiac Regeneration, ventricular remodeling and recovery of mechanical function

Recent studies in animal models of chronic myocardial infarction (*Rota M et al. 2008*) have documented a negative impact of the scarred myocardium on the migration and engraftment of CPCs when compared with acute infarcts. Yet, GF-activated CPCs retain the ability to infiltrate the scar, digest part of the connective tissue, and form cardiomyocytes and coronary vessels via enhanced activity of metalloproteases. In support of these findings (*Rota M et al. 2008*), we showed that HGF and IGF-1

administration triggered the proliferation and mobilization of CPCs, leading to newly formed functionally competent myocardial tissue. Importantly, proliferating myocytes expressed N-Cadherin and Cx43 and linearly increased with the amount of cell loss. Coronary arterioles and capillary structures were concurrently produced with myocytes, tending to preserve blood supply and oxygen diffusion to the surrounding cells. Ultimately, GF-induced activation of CPCs elicited a sustained regenerative response that resulted in a 20% rescue of the infarct by replacing fibrotic tissue with viable myocardium. GF treatment attenuated ventricular dilation, increased ventricular mass/chamber volume ratio, and reduced collagen accumulation in the spared myocardium more than 2-fold while restraining the hypertrophic response of myocytes to the segmental loss of cells.

As shown by the echocardiography findings, post-MI ventricular dysfunction tended to recover in GF treated infarcts. Furthermore, echocardiographic and hemodynamic data documented that the significant, negative correlation of cardiac mechanical function with the extension of the infarcted area in untreated animals was lost as a result of intramyocardial injection of GFs.

It could be argued that a single injection of cells or GFs hardly promotes a sustained and prolonged cardiac repair in the absence of a robust activation of autocrine/paracrine processes. Moreover, the question remains as to whether a 20% recovery of myocardial mass within the infarct, mostly consisting of small contractile cells, is sufficient to prevent the evolution of myocardial infarction toward cardiac decompensation. However, infarct size is proportional to the number of lost cardiomyocytes, representing the major determinant of unfavorable LV remodeling and its chronic evolution toward heart failure (*Olivetti G et al. 1991*). Hence it is of

relevance that the GF-mediated generation of young functionally competent cardiomyocytes succeeds in making cardiac function and anatomy independent of the amount of tissue lost by the occlusion of the supplying coronary artery. These results suggest that locally delivered GFs, by reversing the hostile microenvironment of scarred myocardium, promote a cardiac repair which is proportional to tissue demand.

B) STUDY ON ACUTE MYOCARDIAL INFARCTION

- High-mobility group box 1 protein (HMGB1)

HMGB1 is a multifunctional protein which has both nuclear and extracellular functions. The protein was originally identified as a nonhistone DNA-binding nuclear protein: it binds DNA in a sequence independent manner and modifies DNA structure to facilitate transcription, replication, and repair (*Bustin M 1999*). More recently, a novel role for HMGB1 as a cytokine was identified. Indeed HMGB1 is a potent mediator of inflammation, it is secreted by activated macrophages in response to pro-inflammatory cytokines (*Limana F et al. 2005*) and released passively from necrotic cells. Furthermore, several lines of evidence demonstrated that the effects of the extracellular HMGB1 are mediated, at least in part, by its binding to the receptor for advanced glycation end products (RAGE), a multiligand receptor of the immunoglobulin super-family. It has been reported that HMGB1 is a strong chemo-attractant and a pro-proliferative molecule for vessel-associated stem cells (mesoangioblasts). HMGB1 was shown to act as a signal of tissue damage and to promote proliferation, migration, and differentiation of several stem cell types (*Degryse B et al. 2001; Palumbo R et al. 2004*). Finally, experimental evidence has been provided that intramyocardial administration of exogenous HMGB1 induces resident cardiac progenitor cell proliferation and differentiation, in the murine infarcted heart (*Limana F et al. 2005).* This effect, mediated at least in part by paracrine mechanisms *(Rossini A et al. 2008*), promotes myocardial regeneration, induces a recovery of LV mechanical function, and partially prevents LV remodeling after coronary artery occlusion.

- Recovery of electrical function

HMGB1 has been reported to have both beneficial and detrimental effects (*Lotze MT et al. 2005)* , and these opposite actions were observed in response to "low" and "high" HMGB1 levels, respectively. In the present study, HMGB1 was administered locally at very low dose (2 µg) which is approximately 1000-fold less than that required to induced septic-shock. In addition, HMGB1 was injected into the heart in a critical time window, before necrosis and the associated endogenous HMGB1 increase occurred.

The results reported here demonstrate that the delivery of HMGB1 into the rat heart at the time of acute ischemia induces a recovery of electrical function as suggested by the decline in the occurrence of stress-induced ventricular arrhythmias. Although further studies are required to better understanding the mechanisms underlying the anti-arrhythmic action of the treatment, in accordance with previous studies (*Limana F et al. 2005; Rossini A et al. 2008*), this result can be at least in part ascribed to the HMGB1-induced cardiac regeneration resulting from CPC activation associated with a proper electro-mechanical integration of the newly formed tissue with the spared ventricular myocardium.

References

1. Alvarez-Dolado M, Pardal R, Garcia-Verdugo JM, et al. Fusion of bone-marrow-derived cells with Purkinje neurons, cardiomyocytes and hepatocytes. Nature. 2003;425:968-973..

2. Anversa P, Nadal-Ginard B. Cardiac chimerism: methods matter. Circulation. 2002;106:e129-e131.

3. Anversa P, Sussman MA, Bolli R. Molecular genetic advances in cardiovascular medicine: focus on the myocyte. Circulation. 2004 ;109:2832-2838.

4. Arvidsson A, Collin T, Kirik D, et al. Neuronal replacement from endogenous precursors in the adult brain after stroke. Nat Med. 2002;8:963-970.

5. Assmus B, Schachinger V, Teupe C, et al. Transplantation of Progenitor Cells and Regeneration Enhancement in Acute Myocardial Infarction (TOPCARE-AMI). Circulation. 2002;106:3009-3017.

6. Balsam LB, Wagers AJ, Christensen JL, et al. Haematopoietic stem cells adopt mature haematopoietic fates in ischaemic myocardium. Nature. 2004;428:668-673.

7. Behfar A, Zingman LV, Hodgson DM, et al. Stem cell differentiation requires a paracrine pathway in the heart. FASEB J. 2002;16:1558-1566.

8. Beltrami AP, Barlucchi L, Torella D, et al. Adult cardiac stem cells are multipotent and support myocardial regeneration. Cell. 2003;114:763-776.

9. Boheler KR, Czyz J, Tweedie D, et al. Differentiation of pluripotent embryonic stem cells into cardiomyocytes. Circ Res 2002;91:189-201.

10. Boyden PA, Jeck CD. Ion channel function in disease. Casrdiovasc Res 1995; 29:312-318

11. Bustin M. Regulation of DNA-dependent activities by the functional motifs of the high-mobility-group chromosomal proteins. Mol Cell Biol. 1999;19:5237–5246.

12. Chamuleau SA, Vrijsen KR, Rokosh DG, et al. Cell therapy for ischaemic heart disease: focus on the role of resident cardiac stem cells. Neth Heart J 2009;17:199- 207.

13. Chang MG, Tung L, Sekar RB, et al. Proarrhythmic potential of mesenchymal stem cell transplantation revealed in an in vitro coculture model. Circulation. 2006;113:1832-1841.

14. Chen HS, Kim C, Mercola M. Electrophysiological challenges of cell-based myocardial repair. Circulation 2009;120:2496-2508.

15. Chien KR. Stem cells: lost in translation. Nature. 2004;428:607-608.

16. Clarke DL, Johansson CB, Wilbertz J, et al. Generalized potential of adult neural stem cells. Science. 2000;288:1660-1663.

17. Condorelli G, Borello U, De Angelis L, et al. Cardiomyocytes induce endothelial cells to trans-differentiate into cardiac muscle: implications for myocardium regeneration. Proc Natl Acad Sci U S A. 2001;98:10733-10738.

18. Davis DR, Kizana E, Terrovitis J, et al. Isolation and expansion of functionally-competent cardiac progenitor cells directly from heart. J Mol Cell Cardiol 2010; 49:312-321.

19. Dawn B, Stein AB, Urbanek K, et al. Cardiac stem cells delivered intravascularly traverse the vessel barrier, regenerate infarcted myocardium, and improve cardiac function. Proc Natl Acad Sci U S A 2005;102:3766-3771

20. Degryse B, Bonaldi T, Scaffidi P, et al. The high mobility group (HMG) boxes of thenuclear protein HMG1 induce chemotaxis and cytoskeleton reorganization in rat smooth muscle cells. J Cell Biol. 2001;152:1197–1206.

21. Dimmeler S, Zeiher AM, Schneider MD. Unchain my heart: the scientific foundations of cardiac repair. J Clin Invest 2005;115:572-583.

22. Dodge HT, Baxley WA. Left ventricular volume and mass and their significance in heart disease. Am J Cardiol 1969;23:528-537.

23. Duffy HS. Cardiac Connections-The Antiarrhythmic Solution? N Engl J Med 2008;358:1397-1398.

24. Fallon J, Reid S, Kinyamu R, et al. In vivo induction of massive proliferation, directed migration, and differentiation of neural cells in the adult mammalian brain. Proc Natl Acad Sci U S A. 2000;97:14686-14691.

25. Fozzard HA, Schoenberg M. Strength-duration curves in cardiac Purkinje fibres: effects of liminal length and charge distribution. J Physiol. 1972;226:593-618

26. Fozzard HA. Gap junctions and liminal length in hypertrophy: something old and something new. J Cardiovasc Electrophysiol. 2001;12:836-837.

27. Fuchs E, Segre JA. Stem cells: a new lease on life. Cell. 2000;100:143-155.

28. Fukushima S, Varela-Carver A, Coppen SR, et al. Direct intramyocardial but not intracoronary injection of bone marrow cells induces ventricular arrhythmias in a rat chronic ischemic heart failure model. Circulation 2007;115:2254-2261.

29. Fuller MS, Sándor G, Punske B, et al. Estimates of repolarization dispersion from electrocardiographic measurements. Circulation 2000;102:685-691.

30. G Gheorghiade M, Bonow RO. Chronic heart failure in the United States: a manifestation of coronary artery disease. Circulation .1998; 97:282-289.

31. Gepstein L, Ding C, Rehemedula D, et al. In vivo assessment of the electrophysiological integration and arrhythmogenic risk of myocardial cell transplantation strategies. Stem Cells 2010;28:2151-2161.

32. Hahn JY, Cho HJ, Kang HJ, et al. Pre-treatment of mesenchymal stem cells with a combination of growth factors enhances gap junction formation, cytoprotective effect on cardiomyocytes, and therapeutic efficacy for myocardial infarction. J Am Coll Cardiol 2008;51:933-943.

33. Hierlihy AM, Seale P, Lobe CG. The post-natal heart contains a myocardial stem cell population. FEBS Lett. 2002 ;530:239-243.

34. Horner PJ, Gage FH. Regenerating the damaged central nervous system. Nature. 2000;407:963-970.

35. Jackson KA, Majka SM, Wang H,et al. Regeneration of ischemic cardiac muscle and vascular endothelium by adult stem cells. J Clin Invest. 2001;107:1395-1402.

36. Jackson KA, Mi T, Goodell MA. Hematopoietic potential of stem cells isolated from murine skeletal muscle. Proc Natl Acad Sci U S A. 1999;96:14482-14486.

37. Kjekshus J. Arrhythmias and mortality in congestive heart failure. Am J Cardiol. 1990; 65:421–481.

38. Kocher AA, Schuster MD, Szabolcs MJ, et al. Neovascularization of ischemic myocardium by human bone-marrow-derived angioblasts prevents cardiomyocyte apoptosis, reduces remodeling and improves cardiac function. Nat Med. 2001;7:430-436.

39. Kohno, T., Anzai, T., Naito, K., et al. Role of high-mobility group box 1 protein in post-infarction healing process and left ventricular remodelling. Cardiovasc Res 2009; 81, 565−573.

40. Kolettis TM. Arrhythmogenesis after cell transplantation post-myocardial infarction. Four burning questions-and some answers. Cardiovasc Res. 2006;69:299-301.

41. Kondo T, Raff M. Oligodendrocyte precursor cells reprogrammed to become multipotential CNS stem cells. Science. 2000;289:1754-1757.

42. Kuhlmann MT, Kirchhof P, Klocke R, et al. CSF/SCF reduces inducible arrhythmias in the infarcted heart potentially via increased connexin43 expression and arteriogenesis. J Exp Med. 2006, 23;203:87-97.

43. Lagasse E, Connors H, Al-Dhalimy M, et al. Purified hematopoietic stem cells can differentiate into hepatocytes in vivo. Nat Med. 2000;6:1229-1234.

44. Lapicque L. Quantitative investigations of electrical nerve excitation treated as polarization. Biol Cybern 2007;97:341-349.

45. Laugwitz KL, Moretti A, Lam J, et al. Postnatal isl1+ cardioblasts enter fully differentiated cardiomyocyte lineages. Nature 2005; 433:647-653.

46. Leri A, Kajstura J, Anversa P. Cardiac stem cells and mechanisms of myocardial regeneration. Physiol Rev 2005;85:1373-1416..

47. Limana F, Zacheo A, Mocini D, et al. Identification of myocardial and vascular precursor cells in human and mouse epicardium. Circ Res 2007; 101:1255-1265.

48. Limana F., Germani A., Zacheo A., et al. Exogenous high-mobility group box 1 protein induces myocardial regeneration after infarction via enhanced cardiac C-kit+ cell proliferation and differentiation. Circulation Research 2005;97:73–83.

49. Linke A, Müller P, Nurzynska D, et al. Stem cells in the dog heart are self-renewing, clonogenic, and multipotent and regenerate infarcted myocardium, improving cardiac function. Proc Natl Acad Sci U S A. 2005;102:8966-8971.

50. Lotze MT, Tracey KJ. High-mobility group box 1 protein (HMGB1): nuclear weapon in the immune arsenal. Nat Rev Immunol. 2005;5:331–342.

51. Lux RL, Gettes LS, Mason JW. Understanding proarrhythmic potential in therapeutic drug development: alternate strategies for measuring and tracking repolarization. J Electrocardiol 2006;39:161-164.

52. Ly HQ, Nattel S. Stem cells are not proarrhythmic: letting the genie out of the bottle. Circulation 2009;119:1824-1831.

53. Macchi E, Cavalieri M, Stilli D, et al. High-density epicardial mapping during current injection and ventricular activation in rat hearts. Am J Physiol Heart Circ Physiol 1998;275:1886-1897.

54. Macia E, Boyden PA. Stem cell therapy is proarrhythmic. Circulation 2009;119:1814-1823.

55. Makkar RR, Lill M, Chen PS. Stem cell therapy for myocardial repair: is it arrhythmogenic? J Am Coll Cardiol. 2003;42:2070-2072.

56. Malik M, Camm AJ. Heart rate variability. Armonk, NY: Futura Publishing Co.; 1995

57. Malouf NN, Coleman WB, Grisham JW, et al. Adult-derived stem cells from the liver become myocytes in the heart in vivo. Am J Pathol. 2001;158:1929-1935.

58. Marbán E, Cheng K. Heart to heart: The elusive mechanism of cell therapy. Circulation. 2010;121:1981-1984

59. Marionneau C, Brunet S, Flagg TP, et al. Distinct cellular and molecular mechanisms underlie functional remodeling of repolarizing K^+ currents with left ventricular hypertrophy. Circ Res 2008;102:1406-1415.

60. Martin CM, Meeson AP, Robertson SM, et al. Persistent expression of the ATP-binding cassette transporter, Abcg2, identifies cardiac SP cells in the developing and adult heart. Dev Biol 2004; 265:262-275.

61. Martinez M, Calvo Torrent A, Pico Alfonso MA. Social defeat and subordination as models of social stress in laboratory rodents: a review. Aggress Behav 1998;24:241-256.

62. Menasche P, Hagege AA, Scorsin M, et al. Myoblast transplantation for heart failure. Lancet. 2001;357:279-280.

63. Menasche P, Hagege AA, Vilquin JT, et al. Autologous skeletal myoblast transplantation for severe postinfarction left ventricular dysfunction. J Am Coll Cardiol. 2003;41:1078-1083.

64. Messina E, De Angelis L, Frati G, et al. Isolation and expansion of adult cardiac stem cells from human and murine heart. Circ Res 2004; 95:911-921.

65. Mills WR, Mal N, Kiedrowski MJ, et al. Stem cell therapy enhances electrical viability in myocardial infarction. J Mol Cell Cardiol 2007;42:304-314.

66. Mitchell GF, Jeron A, Koren G. Measurement of heart rate and Q-T interval in the conscious mouse. Am J Physiol Heart Circ Physiol 1998;274:747-751.

67. Monje ML, Mizumatsu S, Fike JR, et al. Irradiation induces neural precursor-cell dysfunction. Nat Med. 2002;8:955-962.

68. Murry CE, Soonpaa MH, Reinecke H, et al. Haematopoietic stem cells do not transdifferentiate into cardiac myocytes in myocardial infarcts. Nature. 2004;428:664-668.

69. Nygren JM, Jovinge S, Breitbach M, et al. Bone marrow-derived hematopoietic cells generate cardiomyocytes at a low frequency through cell fusion, but not transdifferentiation. Nat Med. 2004;10:494-501.

70. Ogawa S, Furuno I, Satoh Y, et al. Quantitative indices of dispersion of refractoriness for identification of propensity to re-entrant ventricular tachycardia in a canine model of myocardial infarction. Cardiovasc Res 1991;25:378-383

71. Oh H, Bradfute SB, Gallardo TD, et al. Cardiac progenitor cells from adult myocardium: homing, differentiation, and fusion after infarction. Proc Natl Acad Sci U S A. 2003;100:12313-12318.

72. Olivetti G, Capasso JM, Meggs LG, et al. Cellular basis of chronic ventricular remodeling after myocardial infarction in rats. Circ Res 1991;68:856-869.

73. Opthof T, Coronel R, Vermeulen JT, et al. Dispersion of refractoriness in normal and ischaemic canine ventricle: effects of sympathetic stimulation. Cardiovasc Res 1993;27:1954-1960.

74. Orlic D, Hill JM, Arai AE. Stem cells for myocardial regeneration. Circ Res. 2002;91:1092-1102.

75. Orlic D, Kajstura J, Chimenti S, et al. Bone marrow cells regenerate infarcted myocardium. Nature. 2001a;410:701-705.

76. Orlic D, Kajstura J, Chimenti S, et al. Mobilized bone marrow cells repair the infarcted heart, improving function and survival. Proc Natl Acad Sci 2001b;98:10344-10349

77. Orlic D, Kajstura J, Chimenti S, et al. Transplanted adult bone marrow cells repair myocardial infarcts in mice. Ann N Y Acad Sci. 2001c;938:221-229.

78. Pak HN, Qayyum M, Kim DT, et al. Mesenchymal stem cell injection induces cardiac nerve sprouting and increased tenascin expression in a swine model of myocardial infarction. J Cardiac Electrophysiol 2003;14:841-848.

79. Palumbo R, Sampaolesi M, De Marchis F, et al. Extracellular HMGB1, a signal of tissue damage, induces mesoangioblast migration and proliferation. J Cell Biol. 2004;164:441–449.

80. Perin EC, Dohmann HF, Borojevic R, et al. Transendocardial, autologous bone marrow cell transplantation for severe, chronic ischemic heart failure.Circulation. 2003;107:2294-2302.

81. Peters NS, Coromilas J, Severs NJ, et al. Disturbed Connexin43 gap junction distribution correlates with the location of reentrant circuits in the epicardial border zone of healing canine infarcts that cause ventricular tachycardia. Circulation 1997; 95:988-996

82. Pinto JM, Boyden PA. Electrical remodeling in ischemia and infarction. Cardiovasc res 1999; 42:284-297.

83. Quaini F, Urbanek K, Beltrami AP, et al. Chimerism of the transplanted heart. N Engl J Med. 2002;346:5-15.

84. Reynolds BA, Weiss S. Generation of neurons and astrocytes from isolated cells of the adult mammalian central nervous system. Science. 1992;255:1707-1710.

85. Roell W, Lewalter T, Sasse P, et al. Engraftment of connexin 43-expressing cells prevents post-infarct arrhythmia. Nature. 2007;450:819-824.

86. Rossini A., Zacheo A., Mocini D., et al. HMGB1-stimulated human primary cardiac fibroblasts exert a paracrine action on human and murine cardiac stem cells. Journal of Molecular and Cellular Cardiology 2008;44:683–693.

87. Rota M, Padin-Iruegas ME, Misao Y, et al. Local activation or implantation of cardiac progenitor cells rescues scarred infarcted myocardium improving cardiac function. Circ Res. 2008;103:107-116.

88. Sgoifo A, Stilli D, Medici D, et al. Electrode positioning for reliable telemetry ECG recordings during social stress in unrestrained rats. Physiol Behav 1996;60:1397-1401.

89. Shi D, Reinecke H, Murry CE, et al. Myogenic fusion of human bone marrow stromal cells, but not hematopoietic cells. Blood. 2004;104:290-294.

90. Smith RR, Barile L, Messina E, et al. Stem cells in the heart: what's the buzz all about? Part 2: Arrhythmic risks and clinical studies. Heart Rhythm 2008;5:880-887.

91. Smith WTt, Fleet W, Johnson TA, et al. The Ib phase of ventricular arrhythmias in ischemic in situ porcine heart is related to changes in cell-to-cellelectrical coupling. Circulation 1995; 92:3051-3060

92. Smits PC, van Geuns RJ, Poldermans D, et al. Catheter-based intramyocardial injection of autologous skeletal myoblasts as a primary treatment of ischemic heart failure: clinical experience with six-month follow-up. J Am Coll Cardiol. 2003;42:2063-2069.

93. Spees JL, Olson SD, Ylostalo J, et al. Differentiation, cell fusion, and nuclear fusion during ex vivo repair of epithelium by human adult stem cells from bone marrow stroma. Proc Natl Acad Sci U S A. 2003;100:2397-2402.

94. Stamm C, Westphal B, Kleine HD, et al. Autologous bone-marrow stem-cell transplantation for myocardial regeneration. Lancet. 2003;361:45-46.

95. Stilli D, Berni R, Bocchi L, et al. Vulnerability to ventricular arrhythmias and heterogeneity of action potential duration in normal rats. Exp Physiol. 2004;89:387-396.

96. Stilli D, Lagrasta C, Berni R, et al. Preservation of ventricular performance at early stages of diabetic cardiomyopathy involves changes in myocyte size, number and intercellular coupling. Basic Res Cardiol 2007;102:488-499.

97. Strauer BE, Brehm M, Zeus T, et al. Intracoronary, human autologous stem cell transplantation for myocardial regeneration following myocardial infarction. Dtsch Med Wochenschr. 2001;126:932-938.

98. Taccardi B, Punske BB, Macchi E, et al. Epicardial and intramural excitation during ventricular pacing: effect of myocardial structure. Am J Physiol Heart Circ Physiol 2008;294:1753-1766.

99. Terada N, Hamazaki T, Oka M, et al. Bone marrow cells adopt the phenotype of other cells by spontaneous cell fusion. Nature. 2002;416:542-545.

100. Tozakidou M, Goltz D, Hagenström T, et al. Molecular and functional remodeling of $I_{(to)}$ by angiotensin II in the mouse left ventricle. J Mol Cell Cardiol. 2010;48:140-151.

101. Tse HF, Kwong YL, Chan JK, et al. Angiogenesis in ischaemic myocardium by intramyocardial autologous bone marrow mononuclear cell implantation. Lancet. 2003;361:47-49.

102. Urbanek K, Quaini F, Tasca G, et al. Intense myocyte formation from cardiac stem cells in human cardiac hypertrophy. Proc Natl Acad Sci U S A. 2003;100:10440-10445.

103. Urbanek K, Rota M, Cascapera S, et al. Cardiac stem cells possess growth factor-receptor systems that after activation regenerate the infarcted myocardium, improving ventricular function and long-term survival. Circ Res. 2005;97:663-673.

104. van der Heyden M.A., Wijnhoven T.J. Opthof T. Molecular aspects of adrenergic modulation of the transient outward current, Cardiovasc. Res. 2006;71:430-442.

105. van Rijen HV, van Veen TA, Gros D, Wilders R, et al. Connexins and cardiac arrhythmias. Adv Cardiol 2006;42:150-160.

106. Vassilopoulos G, Wang PR, Russell DW. Transplanted bone marrow regenerates liver by cell fusion. Nature. 2003;422:901-904.

107. Walker MJA, Curtis MJ, Hearse DJ, et al. The Lambeth Conventions: guidelines for the study of arrhythmias in ischaemia infarction, and reperfusion. Cardiovasc Res 1988;22:447-455.

108. Wang D, Zhang F, Shen W, et al. Mesenchymal stem cell injection ameliorates the inducibility of ventricular arrhythmias after myocardial infarction in rats. Int J Cardiol Epub of print 2010 (DOI: 10.1016/j.ijcard.2010.07.025) .

109. Wang X, Willenbring H, Akkari Y,et al. Cell fusion is the principal source of bone-marrow-derived hepatocytes. Nature. 2003;422:897-901.

110. Wit AL, Janse MJ The ventricular arrhythmias of ischemia and infarction. Futura Publishing Company, Inc, Mount Kisco New York, 1993

111. Ying QL, Nichols J, Evans EP, et al. Changing potency by spontaneous fusion. Nature 2002;416:545-548.

112. Zhang YM, Hartzell C, Narlow M, et al, Stem cell-derived cardiomyocytes demonstrate arrhythmic potential. Circulation 2002,106:1294-1299.